MULTI-SCALE COMPUTATION IN HEMODYNAMICS

By

NARCISSE ABOU N'DRI

A DISSERTATION PRESENTED TO THE GRADUATE SCHOOL
OF THE UNIVERSITY OF FLORIDA IN PARTIAL FULFILLMENT
OF THE REQUIREMENTS FOR THE DEGREE OF
DOCTOR OF PHILOSOPHY

UNIVERSITY OF FLORIDA

2002

To Jean-Claude Lelievre,

ACKNOWLEDGMENTS

I would like to thank Dr. Tran-Son-Tay not only for giving me the opportunity to finalize my education in USA but also for helping me since my arrival in Gainesville.

To Dr. Shyy Wei, I would like to extend my appreciation and respect for giving me the possibility to conduct my research in computational fluid dynamics with moving boundaries. As stated by Hobbes, "All thought is a kind of Computation." I thank him for allowing me to discover this challenging field and for all the help and support to achieve this work.

For Dr. Tran-Son-Tay and Dr. Shyy, I would like to quote one of my favorite thoughts, which is "When you follow an elephant, the dew cannot touch you." I thank them again for everything.

I sincerely thank Professor Ulrich Kurzweg, Professor Nicolae Cristescu and Professor Richard Dickinson for serving as members of my supervisory committee.

While we were looking for a post-doctoral position, my former advisor, Jean–Claude Lelievre, decided that it would be better for me to pursue my study in the USA and go for a PhD degree instead. I told him that this would be difficult because of the language barrier. His answer was that when I arrived in France, I had to go through difficulties, but I managed to overcome them, so I can succeed anywhere if I put my mind on it. I thank professor Lelievre for believing in me.

I would like to thank all the colleagues of the computational thermo-fluid group, in particular Marianne Francois, Inanc Senocak, and the colleagues of the cellular mechanics and biorheology group.

I would like to thank Patricia and Mark for all the years spent together. I have a lot to write about Kathleen, but I can summarize it through Boorstin's thought, "So long as man marked his life only by the cycles of nature--the changing seasons, the waxing or waning moon--he remained a prisoner of nature. If he was to go his own way and fill his world with human novelties, he would have to make his own measures of time." I would like also to extend my thanks to her parents, Mr. and Mrs. Anderson.

I would like to thank my Mom, Ipou Madeleine, and my sister, N'Dri Marie, for all the prayers said and moral support given throughout the years I spent in the USA and in France. I thank them also for being there when I needed them the most. I thank my dad, N'Dri Bernard, and my uncle, Ipou Jean, for always being supportive of all decisions I have made through my years of education.

TABLE OF CONTENTS

Page

LIST OF TABLES

LIST OF FIGURES

NOMENCLATURE

a_{cell}	Area of the cell
f_s	Slippage constant
f_b	Force of a bond
F_b	Total force of bonds
k_{fo}	Equilibrium forward reaction rate
k_f	Forward reaction rate
k_{ro}	Equilibrium reverse reaction rate
k_r	Reverse reaction rate
K_bT	Thermal energy (k_b = Boltzmann constant, T = temperature)
N_b	Density of a bond
N_{bo}	Initial bond density
N_l	Ligand density
N_r	Receptor density
R_c	Cell radius
R_t	Number of receptors
U	Inlet Velocity
X_m	Current position of a bond on the membrane
σ	Spring constant
σ_{ts}	Transition spring constant

σ_{ts}	Transition spring constant
λ	Equilibrium length of a bond
γ	Cell surface tension

Abstract of Dissertation Presented to the Graduate School
of the University of Florida in Partial Fulfillment of the
Requirements for the Degree of Doctor of Philosophy

MULTI-SCALE COMPUTATION IN HEMODYNAMICS

By

Narcisse Abou N'Dri

December 2002

Chair: Dr. Tran-Son-Tay Roger
Cochair: Dr. Shyy Wei
Major Department: Mechanical and Aerospace Engineering

Blood flow dynamics involves length scales across vastly different ranges. For example, adhesion of leukocytes to substrate entails dimensions ranging from nm to μm in length. Understanding the adhesive and rheological behavior of these cells is essential not only for describing microcirculatory flow dynamics, but also for understanding their function and behavior in health and disease. Models of cell adhesion do not combine molecular and full cellular information.

In this study, a multi-scale computational approach for studying the adhesion kinetics and the deformation and movement of a cell on a substrate is presented. The cellular level model consists of a continuum representation of the field equations and a moving boundary tracking capability to allow the cell to change its shape continuously.

At the receptor-ligand level, a bond molecule is mechanically represented by a spring and a reversible kinetics model is used to describe the association and dissociation of bonds. Communication between the macro- and micro-scale models is facilitated interactively with iterations between models until both levels approach compatible solution in each time step.

The computational model is assessed using a cell adhering and deforming along the vessel wall under imposed shear flows. It confirms existing numerical and experimental results. In previous studies, the cell was modeled as solid body or a liquid drop. In the case of adhesion, only a small portion of the contact area was allowed to peel away from the wall.

In this study, modeling the cell as a compound drop, we show that the presence of the nucleus increases the bond lifetime. We also show that increasing cell surface tension decreases the bond lifetime and that vessel diameter affects the cell rolling velocity. Furthermore, we find that the peeling time for a uniform inlet boundary condition is higher than that of a pulsatile one. In addition, increasing cell viscosity for a fixed hydrodynamic force increases linearly the critical bond force, whereas increasing cell surface tension inversely decreases it. Finally, we have shown that a non-zero initial bond force increases the peeling time. The present work shows that cell deformability and hydrodynamic flow affect cell adhesion.

CHAPTER 1
MOTIVATION AND INTRODUCTION

Understanding the adhesion and rolling of a white blood cell on the endothelium wall and its impact on the whole cardiovascular system flow and the blood flow through the aorta and its bifurcations motivate this dissertation. Fundamentally, the blood flow through the cardiovascular system is a multi-scale fluid mechanics problem.

Blood dynamics involves length scales across vastly different ranges. An example is provided by leukocyte adhesion to a substrate, which is an important biomedical problem that has been the subject of extensive research. Analyzing the adhesive and rheological behavior of leukocytes is essential not only for describing microcirculatory flow dynamics, but also for understanding cell function and behavior in health and disease. Computational fluid dynamics (CFD) techniques provide us with powerful tools for tackling a variety of problems in engineering involving fluid flow accompanied by mass, momentum and energy transport. These methods have recently been applied to a variety of problems related to hemodynamics, such as cardiovascular and capillary fluid flow, cellular physics, and adhesion dynamics. Computational fluid dynamics techniques are amongst the most powerful tools available to the engineering branches dealing with the motion of fluids and exchange of mass, momentum and energy.

In particular, fluid dynamics studies of the normal circulation and pathogenesis of cardiovascular diseases such as atherosclerosis, thrombosis and aneurysms have been performed by numerous authors.

In large vessels, dynamics of an individual cell and its impact on fluid properties are negligible but it is not the case for small vessels, where the effect is important. The study of the effect of leukocyte adhesion on blood flow in microvessels is of significant interest for understanding the resistance changes in microcirculation. Several computational fluid dynamic studies have been done to understand flow resistance and drag forces due to adhering leukocytes.

Cell adhesion involves receptors, cells, and vessels with dimensions on the order of nm, μm, and cm, respectively. The study of the effect of leukocyte adhesion on blood flow in microvessels is important for understanding the resistance changes in microcirculation (Pedley, 1980; Skalak, 1972; Weiss, 1990). Knowledge of the effects of the adhesion parameters, rheological properties (viscosity and surface tension), and geometry (cell and tube diameters) of the leukocyte on the adhesion process is important for establishing guidelines for the design of drug particle size and receptor density with reference to the residence time required for the drug to be effective. Models proposed previously in the literature (Bell, 1978; Dembo et al., 1988) do not take into account the rheological properties of the leukocyte. Today, these properties have been shown to have substantial effect on the adhesion process (Dong et al., 1999; Dong and Lei, 2000; Hodges and Jensen, 2002).

Multi-scale modeling of blood flow through arteries is important for understanding the physiological functions of the circulatory system and the patho-physiology of disease processes such as atherosclerosis, hypertension and diabetes, as well as for the diagnosis and medical cure of certain cardiovascular diseases. For example, in large arteries with diameters ranging from 3 cm down to 1 mm, a change in

the dicrotic wave due to reflection indicates changes in the vessel wall and peripheral elasticity, while the absence of the dicrotic wave indicates that the patient may suffer from diabetes or hypertension. Thus, severe artery stenoses (constrictions) can be diagnosed by measuring the pulse wave propagation and reflection in terms of blood pressure or heart sounds. In addition, the location of artery disorders (atherogenesis) correlates with the spatial or temporal distributions of shear stresses exerted by the macroscopic blood flow on the artery vessel wall (Fry,1987; Giddens et al., 1993; Jin et al., 2001; Kilner et al., 1993), as well as with the microscopic mass transport across the arterial endothelium and within the vessel wall.

Issues spanning from cell surface receptors to blood flow in arteries involve disparate scales, as shown in Figure 1-1. A direct computation encompassing all relevant scales, from large vessels to receptor-ligand interaction is beyond the reach of current and foreseeable computational resources (N'Dri et al., 2002). The multi-scale technique allows us to assess the effect of a reflected wave on the distribution of the flow through the aorta for example. An effective overall model can be devised globally using the lumped (1D) model to estimate the pressure and flow rate at a given location, and locally using the 3D field equations to analyze the detailed fluid flow in a given artery.

Figure 1-2 illustrates the broad range of dimensions involved in hemodynamics. The adhesion of a leukocyte to the endothelium wall involves the deformation of a cell whose length is on the order of micrometers, whereas the adhesion equilibrium bond length involves scales on the order of the nanometers. Blood flows from large arteries whose diameters are on the order of centimeters to capillaries whose diameters are on the

order of a few micrometers. To simulate the adhesion process and blood flow in arteries, a multi-scale modeling approach must be developed.

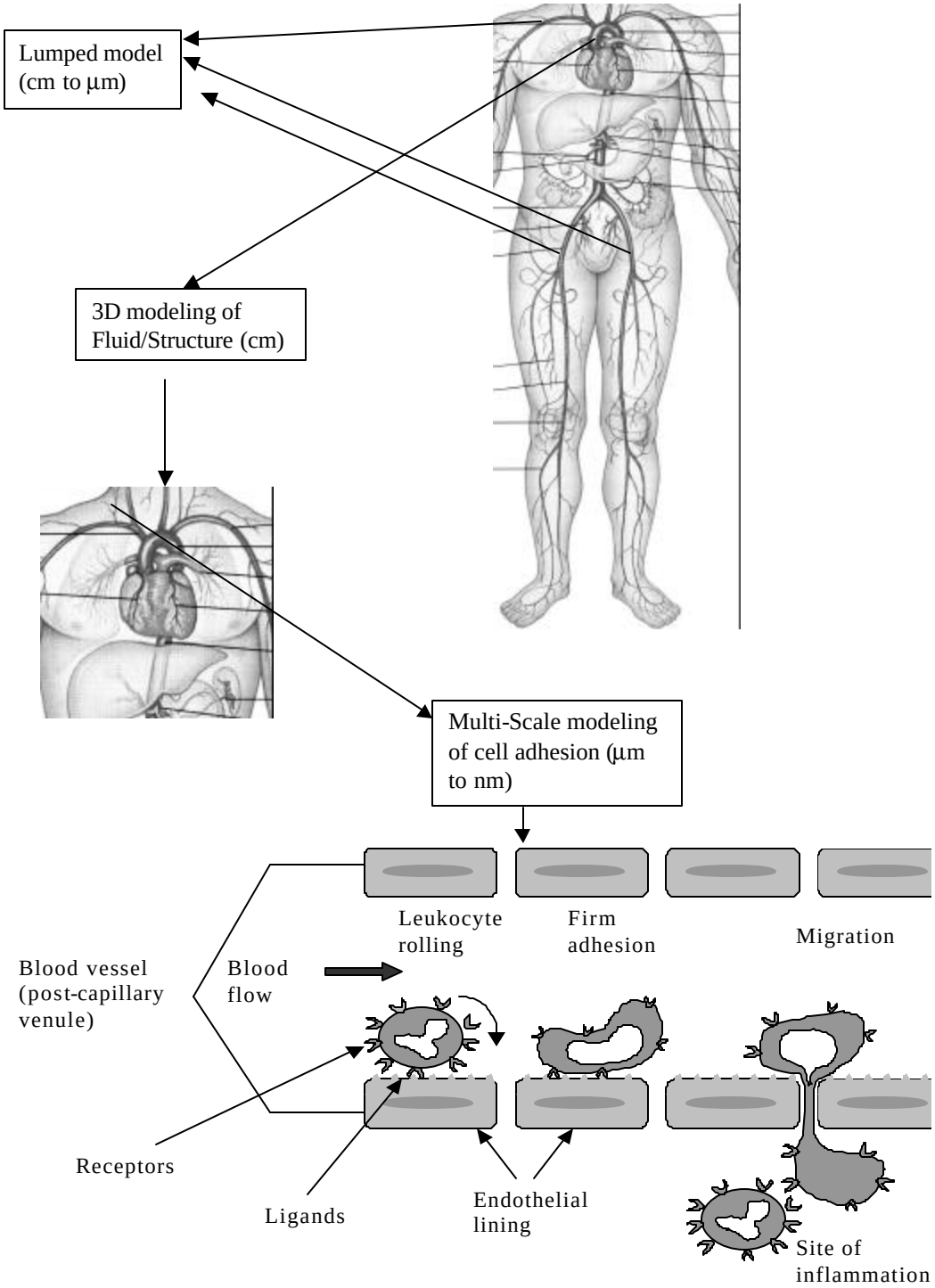

Figure 1-1: Multi-Scale phenomena in hemodynamics. From cellular and/or molecular level to the human cardiovascular system.

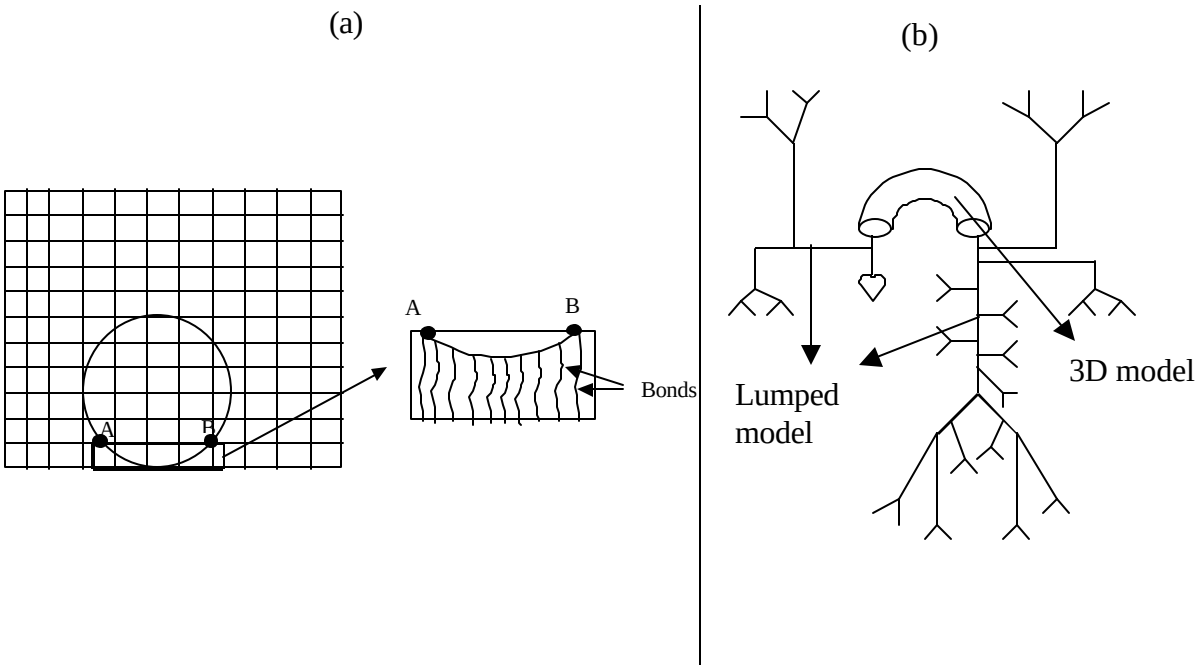

Figure 1-2: Illustration of the multi-scale nature of hemodynamics. (a) Cell adhesion modeling, and (b) 3D flow model and lumped model of the human circulation.

Blood flow through the cardiovascular system is a multi-scale fluid mechanics problem involving flow in arteries, through the capillary network, and in veins. Localized abnormal physiological conditions due to atherogenosis or stenosis can influence the whole network. Change in flow resistance in one vessel will affect the flow in the upstream and downstream branches (Kilner et al., 1993; Liu, 2000). To describe such interactions, the interface between the lumped model and the detailed flow model must be mediated through effective boundary conditions. The multi-scale computation in hemodynamics can be achieved by combining the models at different levels through appropriate interfaces (N'Dri et al., 2002).

The long-term goal of this project is to develop a multi-scale modeling framework spanning form cell surface receptors to blood flow in arteries. However, this is beyond the scope of this dissertation. This study will focus only on the multi-scale modeling of cell deformation and adhesion to provide a starting point for the more challenging multi-

scale problems encountered in the human body. The major computational challenge for the present type of studies is in the treatment of the disparate length scales that exist between cell deformation, whose length scale is on the order of μm, and cell adhesion kinetics, whose length scale is on the order of nm. However, the developed framework will provide a scheme for treating general disparate length scale encounter in engineering problems.

In this dissertation, we will first review the modeling and experimental studies for the leukocyte adhesion in the microvessels, with an overview of the numerical methods used. Then, we will describe the computation technique developed for this work and present the results. Finally, we will provide a discussion of the findings.

CHAPTER 2
REVIEW ON CELL ADHESION

The study of the effect of leukocyte adhesion on blood flow in micro-vessels is of significant interest for understanding the resistance changes in microcirculation.

Adhesion to vascular endothelium (layer of cells lining a blood vessel) is a prerequisite for the circulating leukocytes in order to migrate into tissues. These adhesion events are mediated by coordinated regulation of adhesion molecules expressed by both leukocyte and endothelium. This three-step process is mediated by a series of different endothelial cell-leukocyte adhesion molecules. There are three basic classes of leukocyte-endothelium adhesion molecules: selectins, integrins and immunoglobulins (Long 1995). All the adhesion molecules are membrane proteins.

Significant progress has been made toward understanding the receptor-mediated cell adhesion that is involved in the white blood cell and the endothelium cells interactions (Lauffenburger and Linderman 1993). Detailed experimental studies of the adhesive bonds have suggested that adhesion molecules of the selectin family are involved in maintaining the initial rolling of the leukocytes on the endothelium, whereas the integrin bonds are responsible for firm and prolonged white blood cells attachment to the endothelium cells. The reader is referred to Hammer and Tirrell (1996) for a review of the fundamental parameters that characterize biomolecule function in cell adhesion.

Receptor-mediated cell adhesion plays an important role in many physiological and biotechnological processes.

For example, Springer (1990) shows that leukocyte and tumor cell homing to particular tissues is accomplished by specific receptor interaction with endothelium ligand. The ability to design biomaterial substrate with known and quantifiable densities of adhesion molecules makes it possible to manipulate cell behavior by the correct preparation of the substrate. Kitano et al. (1996) show that bacterial adhesion to biomaterial was prevented by specific blockage of cell adhesion molecule receptors. It is also known that receptor-ligand binding and the resulting adhesion influence cell growth, differentiation, and motility.

Analyzing the effect of leukocyte adhesion on blood flow in micro-vessels is important for understanding flow resistance changes in microcirculation. Adhesion of leukocytes to the blood vessel wall is critical in inflammation (Kaplanski et al., 1993; Lawrence and Springer, 1991) and plays an important role in the function of the immune system (Long, 1995). Rolling of leukocytes under physiological flow is a first step in the migration of cells toward an infection site. Adhesion of a cell to a surface often slows down but does not prevent the cell motion (Alon et al., 1997; Alon et al., 1998). It is facilitated by a complex interaction of receptor-ligand bond formation and dissociation. This initial adhesion is mediated by the P- and E-selectin found on the endothelium surface and by the L-selectin found at the tip of leukocyte microvilli (Hammer and Apte, 1992; Springer, 1990). Blood flow exerts a pulling hydrodynamic force on the adhesion bonds. It has been shown that this pulling force can shorten the adhesion bond lifetime or even extract receptor molecules from the cell surface.

Several models have been proposed for describing the interaction of the leukocyte with the endothelium cells. Mathematical models of cell adhesion can be classified into

two classes based on equilibrium (Evans, 1983; Evans, 1985a) and kinetics concept (Dembo et al., 1988; Hammer and Lauffenburger, 1987). The kinetics approach is more capable of handling the dynamics of cell adhesion and rolling. In this approach, formation and dissociation of bonds occur according to the reverse and forward rate constants. Using this concept, Hammer and Lauffenburger (1987) studied the effect of external flow on cell adhesion. The cell is modeled as a solid sphere, and the receptors at the surface of the sphere are assumed to diffuse and to convect into the contact area, as reviewed by Shyy et al. (2001). The main finding is that the adhesion parameters, such as the reverse and forward reaction rates and the receptor number, have a strong influence on the peeling of the cell from the substrate. Dembo et al. (1988) developed a model based on the ideas of Evans (1985a,b) and Bell (1978). In this model, a piece of membrane is attached to the wall, and a pulling force is exerted on one end while the other end is held fixed. The cell membrane is modeled as a thin inextensible membrane. The model of Dembo et al. (1988) was subsequently extended via a probabilistic approach for the formation of bonds by Cozens-Roberts et al. (1990). Other authors used the probabilistic approach and Monte Carlo simulation to study the adhesion process as reviewed by Zhu (2000). Dembo's model has also been extended to account for the distribution of microvilli on the surface of the cell and to simulate the rolling and the adhesion of a cell on a surface under shear flow. Hammer and Apte (1992) modeled the cell as a microvilli-coated hard sphere covered with adhesive springs. The binding and breakage of bonds and the distribution of the receptors on the tips of the microvilli are computed using a probabilistic approach. Hammer and Apte (1992) studied the effects of the number of receptors, density of ligands, rates of reaction between receptor and ligand,

and stiffness of the receptor-ligand spring on the adhesion of the cell. They also identified their effects on the peeling process. Several minor modifications of these models have been presented, but none takes into account the cell deformability, which has been shown to be necessary for calculating the magnitude of the adhesion force. Table 2-1 summarizes some of the efforts reported in the literature that address the modeling of cell adhesion dynamics. It is clear that much further studies including the role of cell deformation in adhesion are needed. Such knowledge would be particularly helpful in understanding tumor cell adhesion, because metastasizing tumor cells have been reported to deform differently than their non metastasizing counterparts (Weiss, 1990). Dong et al. (1999) and Dong and Lei (2000) have modeled the cell as a liquid drop encapsulated into an elastic ring. They show how the deformability and the adhesion parameters affect the leukocyte and Endothelium cell adhesion process in shear flow. In their study, only a small portion of the adhesion length is allowed to peel away from the vessel wall. This means that their results cannot truly represent what happens in vivo. So a more sophisticated model has to be developed.

Shao and Hochmuth (1996) used the micropipette technique to measure the adhesion bond force and tether formation from neutrophil membrane. They found that a minimum force of 45pN is required for tether formation and the adhesion force increases linearly with the tether velocity. Shao et al. (1998) used the methodology developed by Shao and Hochmuth (1996) to measure the static and dynamic length of neutrophil microvilli. In all their experiments, they found a free motion rebound length, which is independent of the applied suction pressure. An explanation of this behavior is that this length is in fact the natural or static tether length. After the microvillus reaches its

natural length, it will extend under a small pulling force or form a tether under a high pulling force.

Table 2-1: Overview of some fundamental adhesion kinetic models.

Kinetic Model	Main Assumptions/Features	Major Findings
Point Attachment (Hammer and Lauffenberger, 1987)	- Bonds are equally stressed in the contact area (flat) - Binding & dissociation occur according to characteristic rate constants - Receptors diffuse and convect into the binding area of contact	- Adhesion occurrence depends on values of dimensionless quantities that characterize the interaction between the cell and the surface
Peeling (Dembo et al., 1988)	- Clamped elastic membrane - Bond stress and chemical rate constants are related to bond strain - Bonds are linear springs fixed in the plane of the membrane - Chemical reaction of bond formation and breakage is reversible - Diffusion of adhesion molecules is negligible	- Critical tension to overcome the tendency of the membrane to spread over the surface can be calculated - Predictions of model depend whether the bonds are catch-bonds or slip-bonds - If adhesion is mediated by catch-bonds, then no matter how much tension is applied, it is impossible to separate membrane & surface.
Microvilli-coated hard sphere covered w/ adhesive springs (Hammer and Apte, 1992)	-Combined point attachment model with peeling model - Binding determined by a random statistical sampling of a probability distribution that describes the binding (or unbinding)	- Model can describe rolling, transit attachment, firm adhesion - A critical adhesion modulator is the spring slippage (it relates the strain of a bond to its rate of breakage; the higher the slippage, the faster the breakage for the same strain
2D elastic ring (Dong et al. 1999)	- Bond density related to the kinetics of bond formation - Bonds are elastic springs - Interaction between moving fluid & adherent cell	-Shear forces acting on the entire cortical shell of the cell are transmitted on a relatively small “peeling zone” at the cell’s trailing edge

Both microvilli extension and tether formation are found to be important in the rolling of the cell on the endothelium. Extension of the microvillus and formation of a tether can affect the magnitude of the bond force.

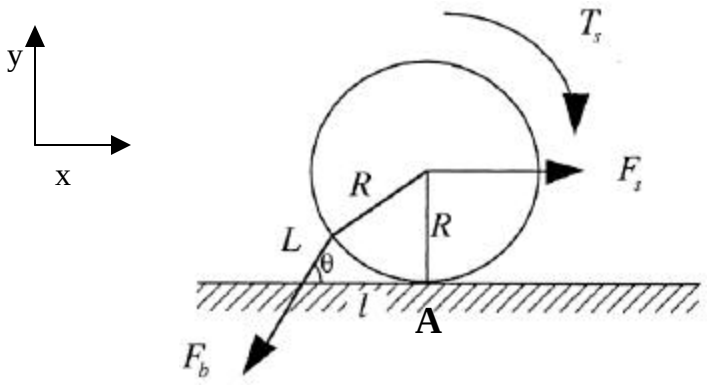

Figure 2-1: Force balance on an adhered neutrophil mediated by a single attachment. L is the total length of the microvillus, l the moment arm length, R the cell radius, F_b the bond force, F_s the force and T_s the shear stress imposed by the shear flow on the cell.

For a microvillus extension, the spring constant derived by Shao et al. (1998) under the assumption that no threshold force exists is 43pN/μm. At low Reynolds number typical of blood flow through the capillaries, inertial effects on the fluid motion are negligible and a solution derived by Goldman et al. (1967b) may be used to compute the force of a single bond (Shao et al., 1998).

Referring to the geometry in Figure 2-1, the angle θ determining the direction of the bond force can be computed as follows:

$$q = \arctan\frac{R}{l} + \arccos\frac{L^2 + l^2}{2L\sqrt{R^2 + l^2}}, \tag{1}$$

where L is the total length of the microvillus, l the moment arm length, and R the cell radius.

A force balance in the x-direction gives

$$F_b \cos q = F_s = 32.05 t R^2, \tag{2}$$

where F_b is the bond force, F_s the force, and τ the imposed shear stress. The bond force is defined as the force on an adhesive bond. A torque balance with respect to point A gives

$$F_b l \sin q = T_s + RF_s = 43.91t\,R^3, \tag{3}$$

where T_s is the torque imposed by the shear flow on the cell.

For the extension of a microvillus, the bond force F_b is given by

$$F_b = k_1(L - L_0), \tag{4}$$

where k_1 is the bond spring constant and L_0 is the initial length of the microvillus. For the formation of a tether formation, F_b is computed as

$$F_b = F_0 + k_2 \frac{dL}{dt}, \tag{5}$$

where F_o is the initial bond force, dL/dt is the velocity at which the tether is pulling away from the wall and k_2 is the change of the spring constant with time. For a neutrophil, k_1 = 43pN/μm, k_2 = 11pN.s/μm and F_0 = 45pN (Shao and Hochmuth, 1996).

Their results show that the bond force decreases in time, and drops 50% in 0.2 s before reaching a plateau. The moment arm and tether length quickly increase within the first 0.2 s, and then slowly increase. Shao and Hochmuth (1999) studied the strength of anchorage of the transmembrane receptors to cytoskeleton, which is believed to be important in cell adhesion and migration. In this experiment, micropipette suction was used to apply force to human neutrophils adhering to latex beads coated with antibodies of the CD626L (L-selectin), CD18 (β_2 integrins), or CD45. The adhesion bond lifetime is defined as the time period between the moment the cell is pulled and the moment the cell resumes its free motion. They computed the pulling force on the cell based on the

theory derived by Shao et al. (1998) as a function of bond lifetime. They found an exponential relationship between the pulling force and the bond lifetime.

$$t = 18e^{-0.085F}, \tag{6}$$

Where F (pN) is the pulling force and τ (s) the bond lifetime.

To explain the rolling of the cells over the endothelium, two mechanisms have been proposed: intrinsic kinetics of bond dissociation (kinetics in the absence of force) and reactive compliance (the susceptibility of the dissociation reaction to an applied force). Leukocytes have been observed to roll faster on L-selectin than on E-selectin and P-selectin. To determine which of these two mechanisms can better describe this difference, Alon et al. (1997) studied the kinetics of tethers and the mechanics of selectin-mediated rolling. Figure 2-2 shows the best fit of their experimental points to the spring model (Dembo et al., 1988), the Bell (1978) equation, and the linear model (Alon et al., 1997). They show that the Bell equation and the spring model both fit the data better than the linear relationship, suggesting an exponential dependence of k_r on F_b. Because the leukocyte is modeled as a rigid body in their force computation, the error in the force computation is estimated to be about $\pm$ 21%, so the computed model constants have to be viewed as an approximation.

Alon et al. (1998) also studied the kinetics of transient and rolling interactions of leukocytes with L-selectin immobilized on a substrate, and measured the rolling velocity for different values of ligand density (L-selectin and P-selectin). For the L-selectin, increasing the ligand density reduces the rolling velocity. The rolling velocity corresponding to the P-selectin is smaller than that of the L-selectin, and there is a threshold shear stress of 0.4 dyn/cm^2 above which rolling can occur.

A frame-by-frame observation performed by Alon et al. (1998) show that leukocytes do not move smoothly on selectin substrates but rather in a jerky fashion. The same behavior was also observed by Chen and Springer (1999).

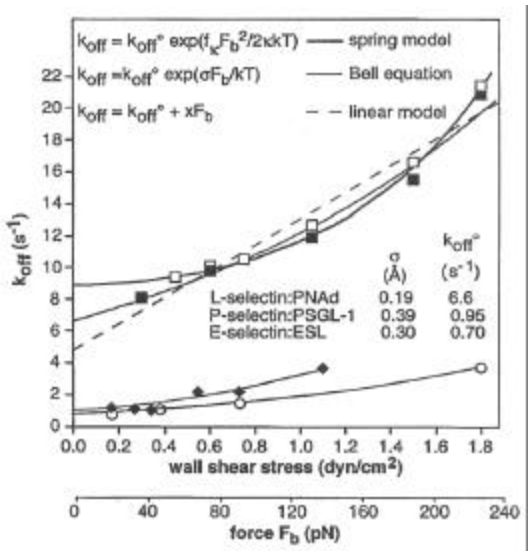

Figure 2-2: Effects of shear stress and Bond force (F_b) on the reverse reaction rate k_{off}^o, also called k_f in text. The solid and dashed lines correspond to the fit to existing models, as displayed in the legend. The squares correspond to L-selectin, the circles to E-selectin, and the rhombus to P-selectin. (Copyright 1998 National academy of Sciences, USA)

Table 2-2: Adhesion parameters computed using Bell and Hookean spring models

		Bell model		Hookean spring model	
Substrate		k_{ro} (s^{-1})	r_0 ($\mathring{A}$)	k_{ro} (s^{-1})	σ/f_σ (N/m)
P-selectin	Smith et and Lawrence (1999)	2.4 ± 0.47	0.39 ± 0.08	3.7 ± 0.51	2.5 ± 0.61
	Alon et al. (1995)	0.93	0.4 ± 0.08	ND	ND
E-selectin	Smith and Lawrence (1999)	2.6± 0.45	0.18 ± 0.03	3.35 ± 0.47	9.12 ± 1.9
	Alon et al. (1995)	0.5-0.7	0.31 ± 0.02	ND	ND
L-selectin	Smith et and Lawrence (1999)	2.8 ± 0.72	1.11 ± 0.12	8.2 ± 0.17	0.9 ± 0.1
	Alon et al. (1997)	7-9.7	0.24 ± 0.02	9.7 ± 0.66	6.31 ± 0.96

The predicted values of the reactive compliance r_0 and reverse reaction rate k_{ro} for L- P- and E-selectins using the Bell equation and σ/f_σ and again k_{ro} using the Hookean model are shown in Table 2-2. A comparison between Smith and Lawrence (1999) and Alon et al. (1997) is also shown. The differences observed in Table 2-2 are due to the type of experimental analysis. In the study of Smith and Lawrence (1999), a high temporal and spatial resolution microscopy is used to allow the capture of features that previous studies could not capture (Alon et al., 1997, 1998).

The effect of the ligand density on the rolling velocity was investigated by Greenberg et al. (2000) who reported an increase of rolling velocity with shear stress and a decrease of the rolling velocity with increasing ligand density. The mean rolling velocity found by Greenberg et al. study lies between 25 to 225 μm/sec. Smith et al. (1999) found that the rolling velocity of a neutrophil rolling over immobilized L-selectin ranges from 50 to 125 μm/sec, while the rolling velocities for P-selectin and E-selectin are 8 μm/sec and 6 μm/sec respectively. The dissociation rate constant k_r is determined from the distribution of pause times observed during leukocyte adhesion, and has been used to quantify the effect of force on bond lifetimes (Kaplanski et al., 1993). By comparing the pause time for neutrophils tethering on P-, E-, L-selectin for estimated bond force ranging from 37 to 250 pN, they found that the pause times for neutrophils interacting with E-selectin or P-selectin are significantly longer than those mediated by L-selectin.

Smith et al. (1999) found that the measured dissociation constants for neutrophil tethering events at 250 pN/bond are lower than the values predicted by the Bell and Hookean spring models. The plateau observed in their graph of the shear stress versus

the reaction rate k_r suggests that there is a force value above which the Bell and spring models are not valid. Since model proposed so far considers the cell as a rigid body, whether the plateau is due to molecular, mechanical or cell deformation is not clear at this time.

Schmidtke and Diamond (2000) studied the interaction of neutrophils with platelets and P-selectin in physiological flow using high-speed, high-resolution video-microscopy. Under wall shear rates ranging from 50 to 300 s^{-1}, an elongated tether is pulled from the neutrophil causing a slight tear-drop-shaped deformation, as seen in Figure 2-3.

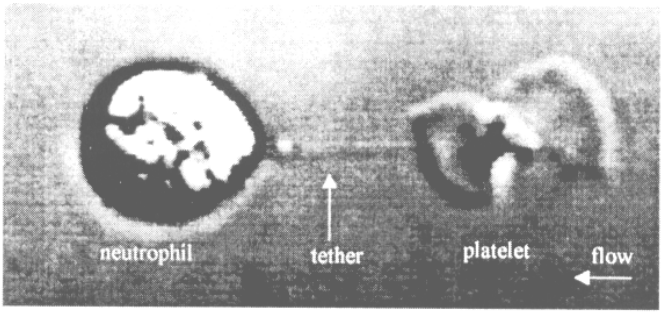

Figure 2-3: Membrane tether formation and tear-drop-shaped deformation. (Reproduced from the journal of cell biology, 2000, vol. 149, pp. 719-729 by copyright permission of the Rockefeller University Press)

The average length of the tether formed by a neutrophil interacting with a spread platelet is estimated to be 5.9 ± 4.1 μm. The average tether lifetime is found to be between 630 and 133 ms for shear rates ranging from 100 s^{-1} (F_b=86pN) to 250 s^{-1} (F_b=172pN), consistent with previous results (Alon et al., 1997; Bell, 1978). Figure 2-4 illustrates the dependence of the tether lifetime on the shear rate.

Schmidtke and Diamond (2000) also studied the rolling of neutrophils over P-selectin-coated surfaces, and observed that when a neutrophil rolls on P-selectin, a tether develops similar to that observed for the spread platelets. The measured tether length and

lifetime are 8.9 ± 8.8 μm and 3.79 ± 3.32 s, respectively. Chang et al. (2000) used computer simulation of cell adhesion to study the initial tethering and rolling process based on Bell's model, and constructed a state diagram for cell adhesion under an imposed shear rate of 100 s^{-1} using the Bell equation shown below

$$k_r = k_{ro} \exp(\frac{r_o f}{k_b T}), \tag{7}$$

where k_{ro} is the unstressed dissociation rate constant, k_bT the thermal energy, r_0 the reactive compliance, and f the bond force.

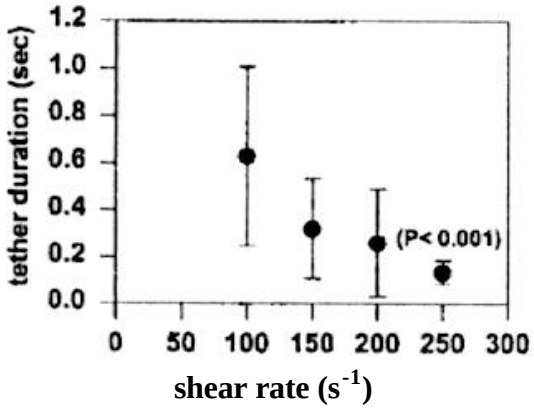

Figure 2-4: Effect of wall shear rate (s^{-1}) on the bond lifetime, P < 0.001 means significant difference for the tether duration. (Reproduced from the journal of cell biology, 2000, vol. 149, pp. 719-729 by copyright permission of the Rockefeller University Press)

Figure 2-5 shows the computed values of k_{ro} as a function of r_0 (γ in the Figure). The symbols correspond to the experimental data obtained for different receptor-ligand pair using the Bell equation. Adhesion occurs for high values of k_{ro} and low values of r_0, as indicated by the wide area between the no-and firm-adhesion zones in Figure 2-5. As r_0 increases, k_{ro} has to decrease in order for adhesion to take place. In the simulation, both association rate k_f and wall shear rate are kept constant. Varying k_f does not change the shape of the state diagram but shifts the location of the rolling envelope in the k_{ro}-r_0

plane. They also found that as the shear rate increases, there is an abrupt change from firm adhesion to no adhesion without rolling motion. For values of r_0 less than 0.1 $\overset{0}{A}$ and high reverse rate constant values k_{ro}, the rolling velocity is independent of the spring constant. A detail on how the computation is performed can be found in N'Dri et al. (2002).

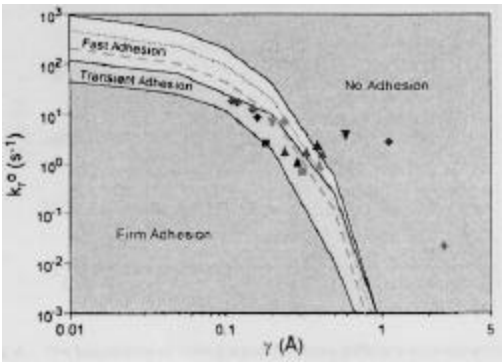

Figure 2-5: State diagram for adhesion. Four different states are shown. The dotted curve represents velocity of 0.3 V_H and the dashed curve represents velocity of 0.1 V_H. The dots correspond to the data listed in Table 2-5 for E-selectin (squares, [Alon et al., 1997, Smith and Lawrence, 1999]), P-selectin (triangles, [Ramachandra et al., 1999, Smith and Lawrence, 1999]), L-selectin (diamonds, [Alon et al., 1998; Chen and Springer, 1999; Ramachandra et al., 1999]). (Copyright 2000 National academy of Sciences, USA)

Tees et al. (2002) used the approach described in Chang et al. (2000) to study the effect of particle size on the adhesion. Three different spherical particles with radii 5.0, 3.75, and 2.5 μm and a shear rate G = 100 s^{-1} are used in their study. The spring constant and the association rate constant were kept fixed. Tees et al. (2002) observed that an increase of the particle size raises the rolling velocity. This is consistent with the experimental finding of Shinde Patil et al. (2001). In both studies (Chang et al., 2000; Tees et al., 2002), the Bell model is used to construct the state diagram but same results can be achieved using the spring model (Dembo et al., 1988). Dong et al. (1999) and Dong and Lei (2000) modeled the cell as a liquid drop encapsulated by an elastic ring and

illustrated the effect of the deformability and adhesion parameters on the interaction between the leukocyte and endothelium in shear flow. Only a small portion of the adhesion length is allowed to peel away from the vessel wall. This constraint is not physically sound, and a more sophisticated model is required.

CHAPTER 3
COMPUTATIONAL METHOD BACKGROUND

The cell adhesion-modeling problem is solved using a fixed Cartesian grid while the interface moves through the mesh, the so-called Eulerian-Lagrangian approach. The advantage of the fixed grid approach is that grid topology remains simple while large distortions of the interface take place. Two approaches can be used to solve this kind of problem. The first one is the Immersed Boundary Technique (IBT) originally used by Peskin (1977) to simulate the heart flow and by Fauci and Peskin (1988) to model the swimming organism, and later extended and applied by, amongst others, (Juric and Tryggvason, 1996; Kan et al., 1998; Udaykumar et al., 1997; Unverdi and Tryggvason, 1992). The second approach is called the Interface Cut-Cell Method (Kwak and Pozrikidis, 1998; Shyy et al., 1996; Ye et al., 1999, 2001). In this dissertation, we will discuss the first approach.

Projection Method

The problem of leukocyte deformation, adhesion and movement is solved using the Navier-Stokes equations. For incompressible flow, these equations are given

Continuity Equation

$$\vec{\nabla}.\vec{u} = 0 \tag{8}$$

Momentum Equation

$$r\left(\frac{\partial \vec{u}}{\partial t} + (\vec{u}.\vec{\nabla})\vec{u}\right) = -\vec{\nabla}p + m\nabla^2\vec{u} + \vec{F} \tag{9}$$

where $\vec{u}$ is the velocity vector, t is the time, p is the pressure, F is the source term, μ is the fluid viscosity and ρ is the fluid density.

Boundary Conditions

Continuity condition

$$(V)_{\text{int}\,erface} = (u.n)_1 = (u.n)_2, \tag{10}$$

Normal stress balance; the dynamic Young-Laplace equation

$$p_2 - p_1 = gk + m_2(\frac{\partial u_n}{\partial n})_2 - m_1(\frac{\partial u_n}{\partial n})_1, \tag{11}$$

where κ is the curvature for two dimensional flows and twice the mean curvature for three dimensional flows, γ is the interfacial tension and n is the normal vector at the interface.

Equations (8-11) are solved using the projection method on a fixed Cartesian collocated grid. The projection method or fractional steps is divided into three steps:

Step 1: Momentum equations solved without pressure

$$\frac{\partial \vec{u}}{\partial t} + (\vec{u}.\vec{\nabla})\vec{u} = n\nabla^2\vec{u} + \vec{F} \tag{12}$$

where ν is the kinematic viscosity.

Step 2: Solve the pressure equation (Poisson type)

$$\begin{cases} \dfrac{\partial \vec{u}}{\partial t} = -\dfrac{1}{r}\vec{\nabla}p \\ \vec{\nabla}.\vec{u} \neq 0 \end{cases} \quad \Rightarrow \quad \vec{\nabla}(\frac{1}{r}\vec{\nabla})p = \frac{1}{\Delta t}\vec{\nabla}.\vec{u} \tag{13}$$

Step 3: Correction step

Numerical Implementation

The convection terms are explicitly treated using the Adams-Bashforth scheme, while the diffusion terms are treated implicitly using the Crank-Nicholson schemes. Both schemes are 2nd order accurate. Figure 3-1 shows the location of the velocity component and the pressure on a grid cell.

Evaluation of the intermediate velocity u_x^* and u_y^* for 2D problem

$$(\frac{\vec{u}^* - \vec{u}^n}{\Delta t}) + (\frac{3(\vec{u}.\vec{\nabla}\vec{u})^n - (\vec{u}.\vec{\nabla}\vec{u})^{n-1}}{2}) = \frac{n\nabla^2\vec{u}^n - n\nabla^2\vec{u}^*}{2} + S \qquad (14)$$

where n is the time step level and S the source term

The pressure equation is derived by assuming that the velocity satisfies the continuity equation at n+1 time step level.

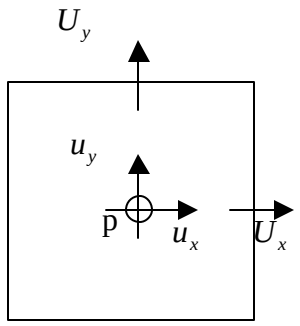

Figure 3-1: velocity and pressure location on a given grid cell

$$\vec{\nabla}.\vec{U}^{n+1} = 0 \quad \Rightarrow \quad \vec{\nabla}.(\frac{1}{r}\vec{\nabla}p^{n+1}) = \frac{1}{\Delta t}\vec{\nabla}.\vec{U}^* \qquad (15)$$

And finally, the correction step is done as follows:

At the cell center:

$$\vec{u}^{n+1} = \vec{u}^* - \Delta t(\frac{1}{r}\vec{\nabla}p^{n+1})_{cc} \qquad (16)$$

At the cell face:

$$\vec{U}^{n+1} = \vec{U}^{*} - \Delta t(\frac{1}{r}\vec{\nabla}p^{n+1})_{fc} \qquad (17)$$

Where cc stands for cell center and fc stands for face cell

Immersed Boundary Technique (IBT)

The IBT approach incorporates the interfacial condition into the field equation without explicitly tracking the interface. As detailed in Udaykumar et al. (1997), the interface can be handled by using markers points. The issues in this approach are the following:

How the interface is represented into the grid domain?

How to treat the material properties jump?

How to communicate the force stored at the interface to the flow field?

How to compute the interfacial velocity once the flow field velocity is known?

How to move the marker point?

Interface Information

The immersed interface is denoted by C(t), the interface is either a curve for 2D problem or a surface for 3D problem. The interface is represented by K marker points of coordinates $\vec{x}_k(s)$ with k=1,….,K and s is the arclength. Figure 3-2 shows the interface numbering and representation. The markers points are regularly separated $0.5h \le ds \le 1.5h$ where h is the grid size. The interface is parameterized as a function of the arclength s by fitting quadratic polynomials $\vec{x}_k(s) = \vec{a}_k s^2 + \vec{b}_k s + \vec{c}_k$ through three consecutive marker points of coordinates $\vec{x}_{k-1}, \vec{x}_k, \vec{x}_{k+1}$. Once the position of the interface is known, the normal and the curvature are evaluated. The convention adopted is that the unit normal point form Fluid 2 to Fluid 1. In 2D the normal is given by:

$$n_x = -\frac{y_s}{\sqrt{x_s^2 + y_s^2}} \quad and \quad n_y = \frac{x_s}{\sqrt{x_s^2 + y_s^2}} \tag{18}$$

Where the subscript s denote d/ds. The curvature is then obtained by taking the divergence of the normal vector

$$k = \vec{\nabla}.\vec{n} \tag{19}$$

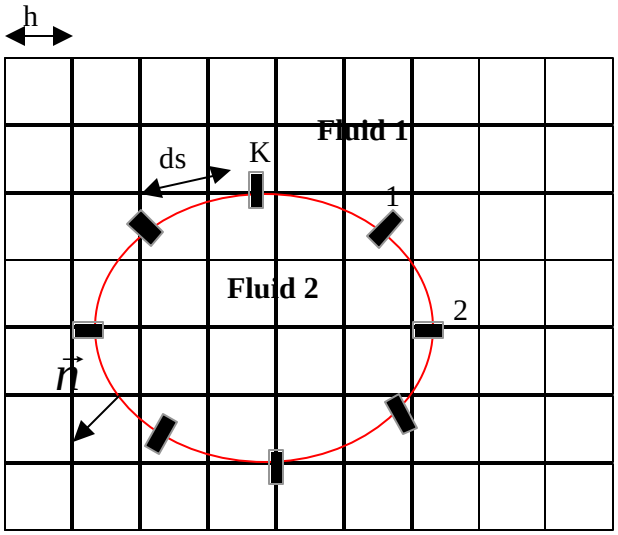

Figure 3-2: Interface representation and numbering

Material Property Assignment

With the known interface position, the material properties are assigned using a Heaviside step function.

$$b = b_1 + (b_2 - b_1)H(\vec{x} - \vec{x}_k) \tag{20}$$

where β is any material property such as density ρ or dynamic viscosity μ. The subscript 1 and 2 denote Fluid 1 and Fluid 2 respectively as shown in Figure 3-2. And $H(\vec{x} - \vec{x}_k)$ is the discrete Heaviside step function defined as follows:

$$H(\vec{x}-\vec{x}_k)=\begin{cases}\prod_{m=1}^{\dim}\frac{1}{2}\left(1+\frac{(\vec{x}_m-(\vec{x}_m)_k)}{d}+\frac{1}{p}\sin\frac{p\,(\vec{x}_m-(\vec{x}_m)_k)}{d}\right) & if\ |\vec{x}-\vec{x}_k|\le d \\ 0 & if\ |\vec{x}-\vec{x}_k|>+d \\ 1 & otherwise\end{cases} \qquad (21)$$

Where dim is the spatial dimension, d=2h with h the grid size, $\vec{x}$ is the grid coordinate and $\vec{x}_k$ is the interfacial point coordinates.

Figure 3-3 shows the definition of the Heaviside function.

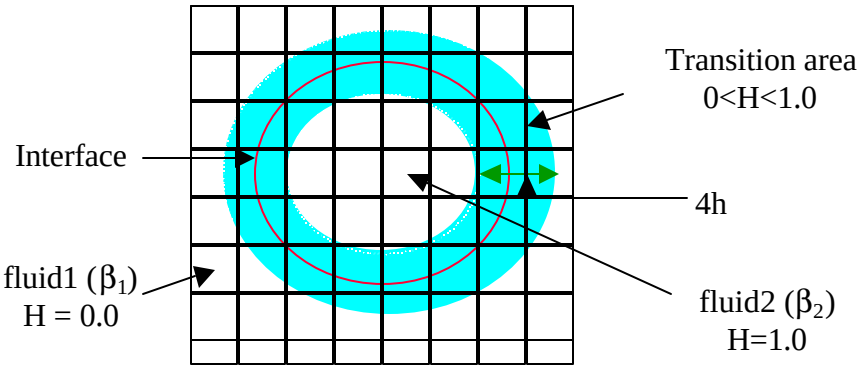

Figure 3-3: Heaviside function definition illustration.

The next step is to communicate the force stored at the interface to the near by grid points.

Source Term Computation

Let recall here the momentum equation $r(\frac{\partial\vec{u}}{\partial t}+(\vec{u}.\vec{\nabla})\vec{u})=-\vec{\nabla}p+m\nabla^2\vec{u}+\vec{F}$

The force $\vec{F}$ exerted by the interface on the flow is transmitted to the momentum equation by means of integral source terms. Here we show this force only on the discretized form:

$$\vec{F}_P=-\sum_k f_k\vec{n}_k d\,(\vec{x}-\vec{x}_k)\Delta s_k \qquad (22)$$

The force at the grip point P is computed based on the sum of the interfacial force f_k of the marker point located inside a circle of radius 2h weighted by the Delta function as shown in Figure 3-4. The delta function is computed as follows and the delta function spreads over 4h and is the derivative of the Heaviside step function.

$$d(\vec{x}-\vec{x}_k)=\begin{cases}\prod_{m=1}^{\dim}\frac{1}{2d}(1+\cos\frac{p(\vec{x}_m-(\vec{x}_m)_k)}{d}) & if\ |\vec{x}-\vec{x}_k|\le d\\ 0 & otherwise\end{cases} \tag{23}$$

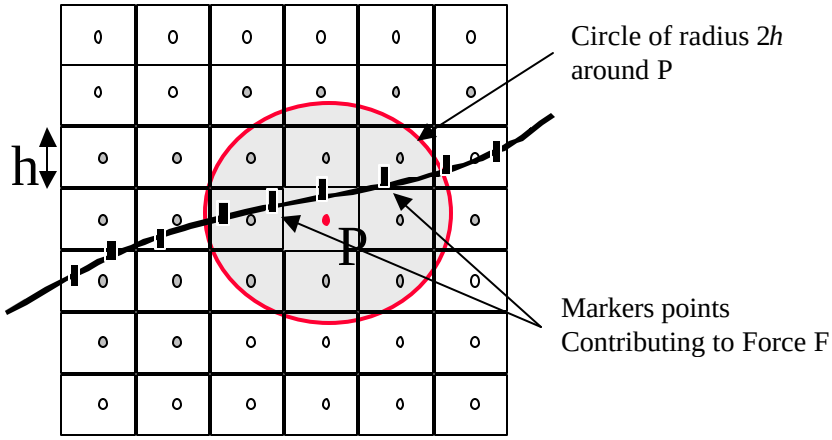

Figure 3-4: Source term computation at the grid point P and marker points contributing to the computation is also shown.

Once the interfacial position is known, the material properties can be assigned properly then the interfacial force is spread to near by grid points and finally the flow field equation can be solved. The next step is to compute the interfacial point velocity.

Interfacial Velocity Computation

The velocity at the marker point is denoted by V_k and should satisfy the continuity condition, so in discretized form the interfacial velocity is:

$$\vec{V}_k=\sum_{ij}\vec{u}_{ij}d(\vec{x}-\vec{x}_k)h^2 \tag{24}$$

Where h is the grid size, i and j are the grid location indices and $\vec{u}$ is the fluid velocity. The computation of the interfacial velocity is illustrated in Figure 3-5. The

velocity is computed by taking the sum of all the grid points located inside a circle of radius 2h.

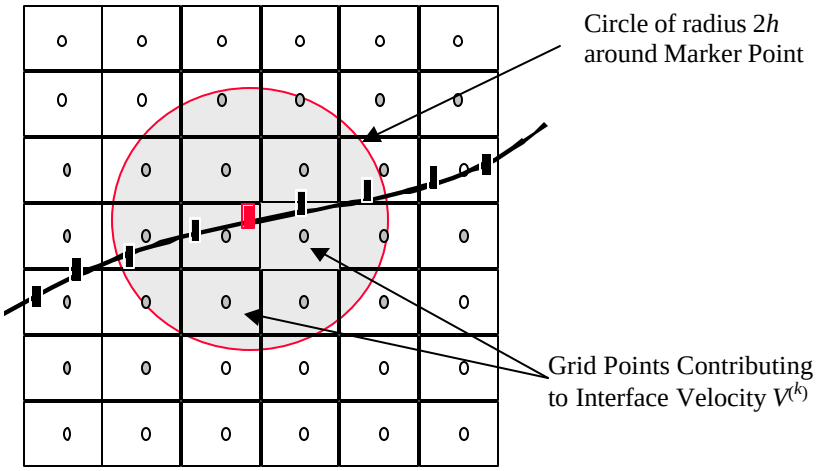

Figure 3-5: Interfacial point velocity computation and grids contributing to the computation is also shown

The last step is the advection of the interface and this is done using the following equation:

$$\vec{x}_k^{n+1} = \vec{x}_k^n + \Delta t(\vec{V}_k^n) \tag{25}$$

This method is used to study the cell adhesion and movement along the endothelium wall.

CHAPTER 4
DEVELOPMENT OF THE MULTI-SCALE METHOD

Although in large vessels, blood cells influence minimally blood flow, they play an important role in flows through small vessels with a lumen diameter comparable to cell size. The ability of a blood cell to deform and flow through capillaries or to migrate in tissues is governed by its mechanical properties. This aptitude to deform is critical to our immune system. The goal here is to develop novel numerical techniques to better understand and predict the effects of a deformable cell in contact with the endothelium, and the force of adhesion between them under quasi-steady sate flow.

Most of the studies of the adhesion were done by assuming a flow over a plate and by using a shear flow at the inlet. But most of the existing experiments are performed using a parallel flow chamber. In addition, in the post capillaries, the diameter of cell and that of the vessel are in the same order; this can affect the rolling of a cell along the vessel wall. Finally, in-vivo the cell is exposed to a pulsatile flow. These flow and geometric characteristics have not been taken into account in previous studies. Furthermore, it has been shown in our laboratory (Kan et al., 1998, 1999a,b) that a compound drop model for the leukocyte reconciles different experiments performed in different laboratories. So in the present a compound drop will be used to study the adhesion of a cell on a substrate.

Model Overview

In order to form a comprehensive modeling framework to treat the disparate

scales between cell deformation (μm) and cell adhesion (nm), a multi-scale model to account for both macroscopic (continuum) and microscopic (ligand-receptor) levels of phenomena is needed.

Recently, N'Dri et al. (2000) have implemented such an approach. In their multi-scale model, the macroscopic component deals with the deformation of the cell and the microscopic part takes care of the adhesion aspect. The continuum scale problem is the one of a fluid flowing over a cell attached to one wall of a tube by an area of contact defined by the membrane segment A-B (Figure 4-1a). The ligand-receptor bond scale problem involves the interaction between the membrane segment A-B and the substrate surface (Figure 4-1b).

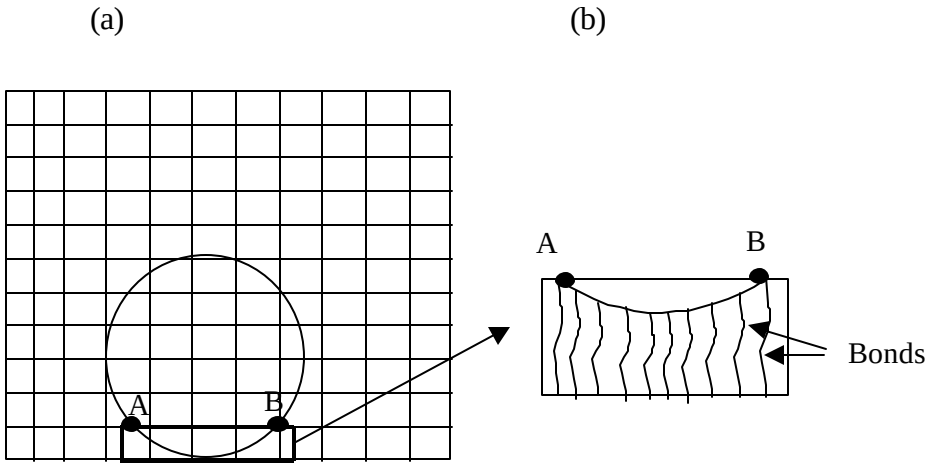

Figure 4-1: Macro-Micro model. The cellular model is shown on the left, whereas the enlarged area on the right shows the micro domain for the receptor model.

Macro-Scale Model

The macroscopic problem consists of a fluid flowing over a cell attached to a flat surface of a tube. Solution to the problem will provide information about the cell shape, velocity, and pressure. That information will be passed to the micro-scale model.

Computation of the source term F

$$F = -\sum_k D(x - X^{(k)})(\gamma k^{(k)} + F_b^{(k)}) n^{(k)} \Delta s^{(k)} \tag{26}$$

Where D is the delta function, γ is the interfacial tension, κ is the curvature, Δs is the arc-length, n is the normal direction vector and F_b is the bond stress which is defined by the micro-scale model.

Micro-Scale Model

The interaction between the cell and surface at the microscopic level is analyzed with the model proposed by Dembo et al. (1988). This model treats a bond as a spring, and the force of a bond, f_b, is given by:

$$f_b = \sigma (x_m - \lambda) \quad and \quad F_b = N_b f_b \tag{27}$$

Where σ is the spring constant, x_m and λ are the current and the equilibrium lengths of a bond, F_b is the total bond force, and N_b is the bond density.

In Dembo's model, major assumptions were made: 1) the bonding stresses are the only distributed stresses acting on the membrane; 2) the bonds are fixed in the plane of the membrane; and 3) the chemical reaction of bond formation and breakage is reversible. Those assumptions have some drawbacks since membrane experience forces due to surrounding forces such as the non specific potential forces, and it is also known that adhesion molecules are able to diffuse laterally in the plane of the membrane. Nonetheless, a significant understanding can be gained from the present study.

Calculation of the bond density, N_b

The balance equation of the formation and dissociation of bonds is given by a simple kinetic relationship:

$$\frac{\partial N_b}{\partial t} = k_f (N_l - N_b)(N_r - N_b) - k_r N_b \tag{28}$$

Where N_b is the bond density, k_r and k_f are the reverse and forward reaction rate coefficients, respectively, N_l is the initial ligand density on the surface, and N_r is the initial density of receptors on the cell membrane.

The reverse and forward reaction rate coefficients are, respectively, given by Dembo et al. (1988):

$$k_r = k_{ro} \exp\left(\frac{(s - s_{ts})(x_m - l)^2}{2k_b T}\right) \tag{29}$$

and

$$k_f = k_{fo} \exp\left(-\frac{s_{ts}(x_m - l)^2}{2k_b T}\right) \tag{30}$$

The initial bond density, N_{bo}, is found by solving the following equation:

$$k_{fo}(N_l - N_{bo})(N_r - N_{bo}) - k_{ro}N_{bo} = 0 \tag{31}$$

Where the subscript o refers to the initial equilibrium state.

The kinetic equation is solved using a 4th order Runge-Kutta method. The micro model has been used to analyze the case of a membrane being pulled away from a surface at a constant velocity (N'Dri et al., 2000; Shyy et al., 2001). The effects of reaction rates, ligand density, and other parameters on the adhesion process have been reported.

Micro-Macro Coupling

The macro-model is first solved to determine the position of the interface while freezing the micro-model. Knowing the position of the interface allows the computation of the actual length of the adhesion molecule. Then, this information is transmitted to the micro-model while freezing the macro-model. The adhesion bond stress is computed in the micro-model and is transmitted to the macro-model via the source term. Information between the two models is continuously exchanged during the course of the computation. The computational flow chart of their approach is shown in Figure 4-2.

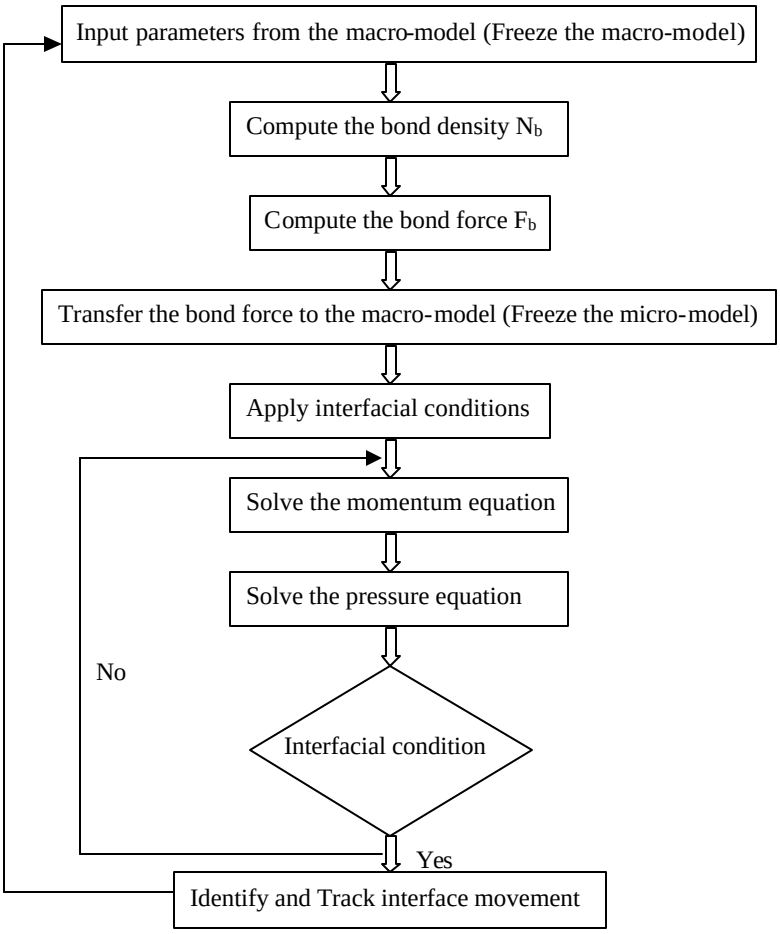

Figure 4-2: Flow chart showing the interaction between the micro-model (receptor scale) and the macro-model (cellular scale).

Macro and Micro Test Cases

In the first part of this study, the macroscopic and the microscopic model were solved separated in order to study the effect of the Reynolds number and the capillary number on the deformation of a cell attached to the wall of a tube and the adhesion parameters such as ligand number, bond stiffness respectively. The main founding of this part of their study can be found in Shyy et al. (2001).

Micro-Scale Test Cases

A cell attached to a wall of a tube is pulled away from the substratum with a

specified velocity, v as indicated in Figure 4-3. The bond is considered disrupted based on the criterion offered by equation $N_{bc} = 10^{-4} N_{bo}$. This computation is conducted to see the effect of the different parameters on the adhesion process.

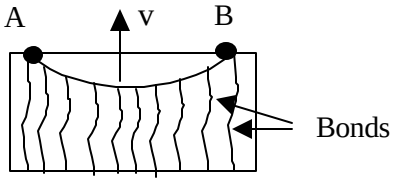

Figure 4-3: Geometry of the test case problem

Figure 4-4 shows the effects of the reverse reaction rate, k_{ro}, on the maximum length of a bond before breaking, for different values of the forward reaction rate k_{fo}. We see that when k_{fo} increases, the maximum length reached by a bond before breaking is greater. For a given value of k_{fo}, the maximum length of a bond decreases as the reverse reaction rate increases. The range of the values of k_{ro} used in this study is $0.1 < k_{ro} < 10 s^{-1}$.

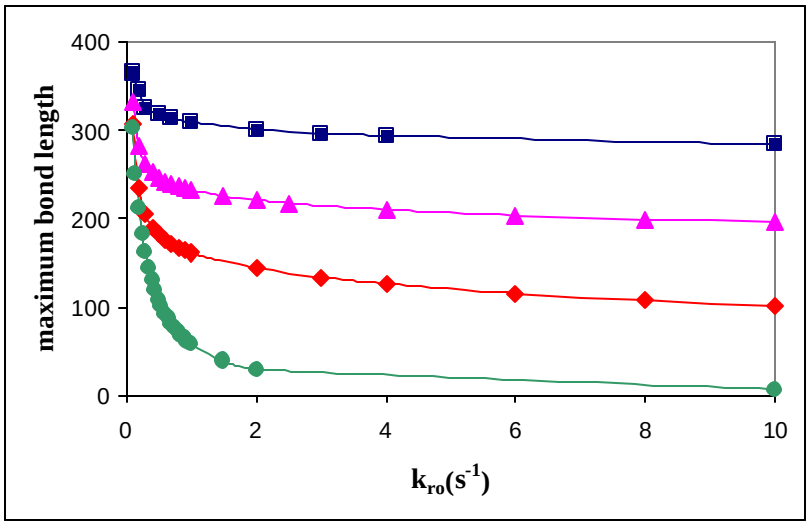

Figure 4-4: Maximum length of a bond before breaking as a function of the reverse reaction rate, for different values of forward reaction rate., (■) for $k_{fo} = 10^{-7} cm^2/sec$, (▲) for $k_{fo} = 10^{-10} cm^2/sec$, (◆) for $k_{fo} = 10^{-12} cm^2/sec$, (●) for $k_{fo} = 10^{-14} cm^2/sec$. The velocity v = 0.1μm/sec.

In all the following figures, v = 0.1μm/sec, k_{fo} = 10^{-14}cm^2/sec, k_{ro} = 0.1s^{-1}, rc = 4×10^{-4} cm, dt = 0.001s, λ = 5×10^{-6} cm, k_bT = 3.8×10^{-7} dyne.cm, N_r = 5×10^{10} cm^{-2}.

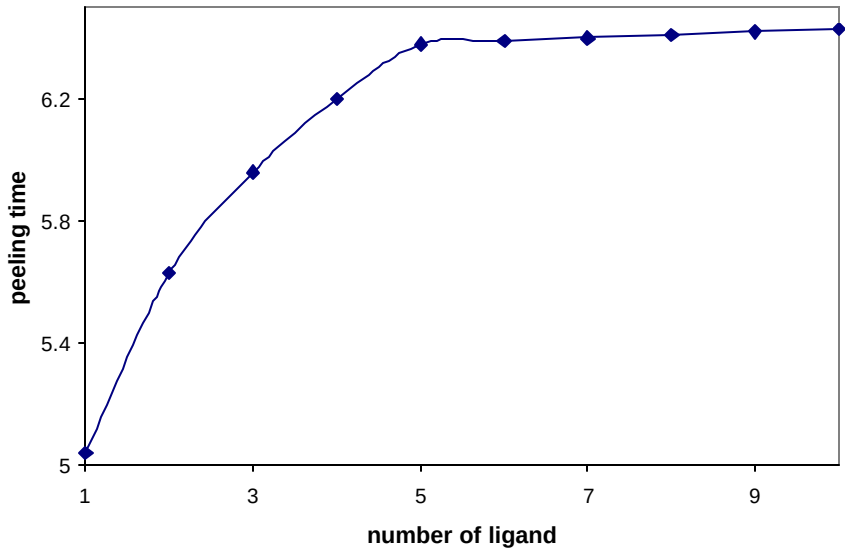

Figure 4-5: Effect of the ligand density (×10^{10}cm^{-2}) on the de-bonding time (s). f_σ=0.1. σ_{ts} = 4.5dyn/cm and σ = 5dyn/cm.

In Figure 4-5, we observe that the de-bonding time increases as the number of the ligand increases. The sharp slope observed at the beginning is due to the fact that the number of ligands is less than the number of receptors, so there are a lot of free receptors at the contact area. Therefore, by increasing the ligand density, the number of bonds increases until the number of ligands outnumbers the number of receptors. At that instant, the bond formation is decreased due to the unavailable receptors at the contact area.

The peeling time decreases as the spring constant increases. The higher the spring constant is the less elastic is the spring and therefore it breaks faster.

Figure 4-6 shows the effect of the slippage constant $f_s = (s-s_{ts})/s$ on the de-bonding time. The slippage constant appears in the computation of the reverse rate reaction (equation 30).

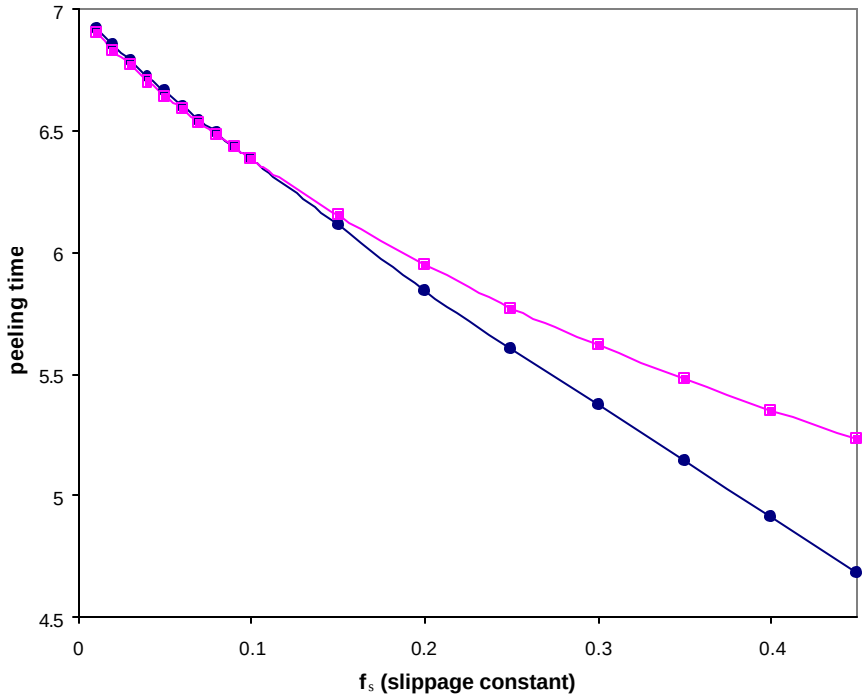

Figure 4-6: Effect of the slippage constant f_s on the de bonding time (s) for σ (circle) and σ_{ts} (square) held constant respectively. The circle dots correspond to σ = 5dyn/cm, and σ_{ts} is allowed to vary with f_s. The square dots correspond to σ_{ts} = 4.5dyn/cm, and σ is allowed to vary with f_σ. $N_r = N_l = 5\times10^{10}$ cm^{-2}.

In this computation, s_{ts} is held constant while s is varying, then s is held constant while s_{ts} is varying. Figure 4-6 shows that f_σ and the peeling time are inversely proportional. When $f_s > 0.1$, the peeling time for s_{ts} is smaller than that of σ constant while for $f_s = 0.1$ the peeling time for fixed value of s_{ts} and s are similar.

Macro-Scale Test Cases

In this section, a droplet adhering to a wall under flow conditions is studied. This computation is done by using equations (8-11). No adhesion molecule is present in this test. In the following computation, the size of the tube is 1.0×2.0, the diameter of the droplet is 0.6, the inlet velocity is taken equal to 1. The properties of the droplet and the surrounding flow are $\mu = 0.01$ Pa.s, $\rho = 1.0$ kg/m^3 and $s = 0.01$ N/m and $s = 0.1$ N/m,

the capillary number $Ca = mU/s = 1.0$ and 0.1 respectively and the Reynolds number $Re = (rUd/m) = 100$. Figure 4-7 shows the instantaneous droplet shapes for two values of the surface tension for a fixed value of the inlet velocity. It is observed that the surface tension has an effect on the shape of the droplet. The droplet shape is smoother for high surface tension.

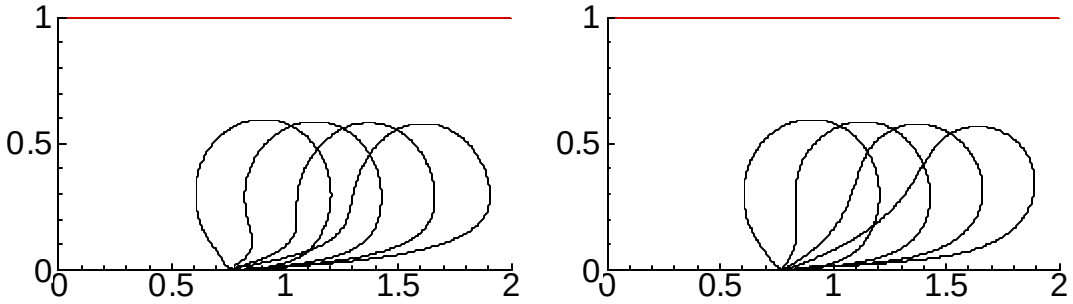

Figure 4-7: Instantaneous droplet shapes for σ = 0.01 N/m (left) and σ = 0.1 N/m (right).

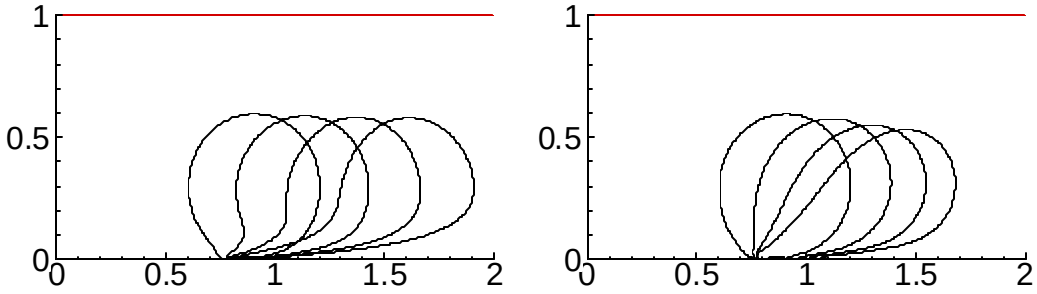

Figure 4-8: Instantaneous droplet shapes for two different values of the droplet viscosity μ = 0.01 Pa.sec (left) and μ = 1.0 Pa.sec (right) and σ = 0.01 N/m for both computations.

The viscosity has a significant effect on the droplet shapes and the flow field velocity as shown by Figure 4-8.

Micro-Macro Coupling

In this paragraph, the interaction of both models was also studied. We will review some of the results for this aspect. An initial membrane shape given by the macro-model is used as the input for the micro-model. The membrane is modeled as a thin inextensible body (Dembo et al., 1988). A difference of pressure across the membrane, based on the

macroscopic solution is applied to find the new position of the membrane. During the first step of this computation, the bond model is not activated. In the next and subsequent time steps, the bond density and force are computed based on the receptor-ligand model. Using this information the new location of the interface is found at every time instant. In the computation, the following values are used: $N_l = N_r = 5.0\times10^{10}$ cm^{-2}, $s = 5.0$ dyne/cm, $s_{ts} = 4.5$dyne/cm, $k_bT = 3.8\times10^{-7}$ dyne.cm.

Instantaneous membrane shapes between points A-B shapes after various time steps are illustrated in Figure 4-9. Again, the initial curve represents the original membrane location segment before a flow is imposed. Initially, due to the action of the hydrodynamic forces, the membrane is pulled away from the substrate. This membrane movement activates the receptor-ligand model, and, consequently, the deformation of the membrane becomes more limited as a higher force is required to deform the bonds. The jump between the initial and first membrane locations in Figure 4-9 is because we didn't start the macroscopic and microscopic models simultaneously. This is done mainly to illustrate the interaction between the two models.

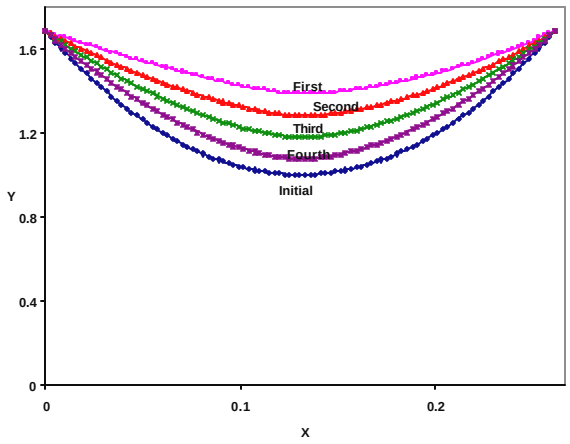

Figure 4-9: Illustration of the instantaneous membrane shape resulting from the pressure field, based on the macroscopic model, and the bond force, based on the receptor-ligand model. The vertical axis is normalized by the bond length, and the horizontal axis by the cell radius.

To understand the behavior observed in Figure 4-9, we plot in Figure 4-10 and Figure 4-11 the variation of the reverse and the forward reaction rates as a function of time.

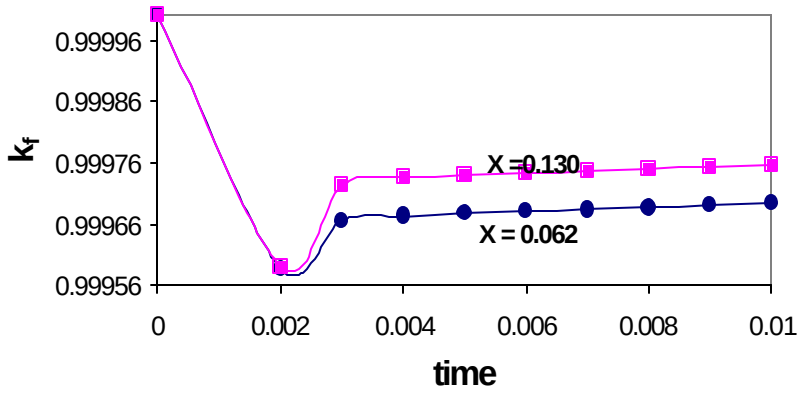

Figure 4-10: Forward reaction rate as a function of time for two different locations of the bonds. X is the abscise of the bond.

The distance between the membrane and the wall has a major impact on the rate constants, as evidenced by Eqs. (29) and (30). Hence, the initial upward movement of the membrane during the first time step, shown in Figure 4-9, is responsible for the initial decrease in the forward rate constant, k_f, in Figure 4-10. The subsequent downward movement of the membrane reverses the trend accordingly. The two curves correspond to the quarter- and half-point of the membrane segments. The above argument is applicable to both forward and reverse rate coefficients, except that the reverse reaction rate coefficient, $k_{r,}$, has an opposite behavior as shown in Figure 4-11.

The main findings of N'Dri et al. (2000) for the kinetic model are:

- The maximum bond length decreases as the reverse reaction rate increases, and increases with an increasing forward reaction rate.
- As the cell velocity increases during the de-bonding process, the maximum bond length increases while the total peeling time decreases.

- The rate of de-bonding decreases as the number of ligands increases.
- The bonds are strong enough to resist the hydrodynamic force generated by a moderate flow and to affect the local shape of the cell membrane.
- The peeling time decreases with increasing spring or slippage constants.
- The peeling time reaches a maximum when the number of ligands equals its receptor counterpart.

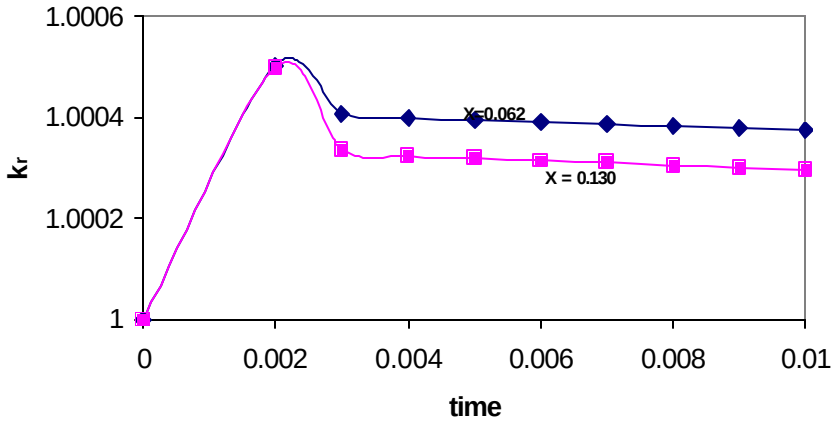

Figure 4-11: Reverse reaction rate as a function of time for two different locations of the bonds. X is the abscise of the bond.

CHAPTER 5
RESULTS

In this chapter, the cell is allowed to deform and to roll along the vessel wall contrary to the precedent computation where the cell remains still during the computation. A 2D dimensional representation of a cell modeled as either simple or compound drop is studied in a planar channel under imposed flow. The cell is attached to one channel wall with adhesive bonds governed by kinetics model proposed by Dembo et al. (1988). A uniform flow is used at the inlet because in vitro experiment uses a parallel flow chamber and in vivo the cell is exposed to a pulsatile flow with a uniform description at a given time. Most of the studies use a shear flow over a plate with cell attached to it. It is also believed that changing the tube or vessel diameter can have an impact on cell adhesion. Furthermore, it has been shown in our laboratory (Kan et al., 1998, 1999a,b) that a compound drop model for the leukocyte reconciles different experiments performed in different laboratories.

Liquid Drop Model

In this paragraph, a two- dimensional cell is attached to a vessel wall, and a uniform flow is imposed at the inlet of the vessel tube as shown in Figure 5-1 in order to study its peeling from the vessel wall using the immersed boundary technique described in Chapter 3. Table 5-1 and Table 5-2 show the adhesion parameters used in the study. All the results presented below will be based on the non-dimensional parametric variations normalized by the reference scales shown in Table 5-3.

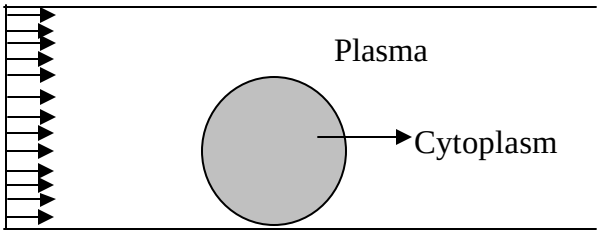

Figure 5-1: Schematic of the problem statement for the simple liquid drop

Table 5-1: Average macro-model parameters.

Tube diameter (μm)	30	Cell viscosity (dyne sec/cm^2)	10-1000
Cell diameter (μm)	6 - 8	Plasma viscosity (dyne sec/cm^2)	1.0
Tube length (μm)	120	Plasma density (g/cm^3)	1.0
U (μm/sec)	50-3200	Interfacial tension (dyne/cm) (Evans, 1983)	10^{-3} – 8.0

Table 5-2: Average micro-model parameters.

Parameter	Value	Parameter	Value
N_r (cm^{-2}) (Bell et al., 1984)	2.0 – 5.0 10^{10}	k_b(dyne.cm/K) (Boltzman Constant)	1.38 10^{-16}
k_{fo} (cm^2/s) (Hammer and Lauffenburger, 1987)	10^{-14}	λ (cm) (Bell et al., 1984)	5.0 10^{-6}
k_{ro} (s^{-1}) (Bell, 1978)	10^{-11}-10	r_c (cm) (Schmid-Shonbein et al., 1980)	4.0 10^{-4}
σ (dyne/cm) (Dembo et al.,1988)	0.5 – 10	$F_\sigma = (\sigma-\sigma_{ts})/\sigma$	0.1
σ_{ts} (dyne/cm) (Dembo et al.,1988)	0.48 – 9.5	N_l (cm^{-2}) (Lawrence and Springer, 1991)	2.0 – 5. 10^{10}

Table 5-3: Reference values used for non-dimensionalization.

Length	30 μm	Viscosity	1 dyne sec/cm^2
Velocity	600 μm/sec	Density	1.0 g/cm^3
Spring constant	5.0dyne/cm	Bond density	5.10^{10}cm^{-2}
Reverse reaction rate	0.1 sec^{-1}	Interfacial tension	0.1 dyne/cm

In all the computations, unless specified otherwise, the values used for k_{fo}, σ, and σ_{ts} are 0.1 s^{-1}, 5 dyne/cm, and 4.5 dyne/cm, respectively. Using these parameters, the effects of the reverse reaction rate, the wall, and the spring constant σ on the

rolling/displacement of the cell along the endothelium are evaluated. The cell is first modeled as a liquid drop with a constant viscosity and surface tension. This is the simplest model one can use to describe qualitatively certain rheological behaviors of leukocytes (Evans and Yeung, 1989). Figure 5-2a shows the instantaneous position of an interfacial point on the cell surface for a given k_{ro}. It is seen that the cell translates along the wall and rotates at the same time. The combination of these two movements leads to the rolling of the cell along the wall. The cell initially rolls along the wall and starts to slide along the vessel wall when the bonds offer no more resistance as shown by the plateau observed in Figure 5-2b. The curve trend can be qualitatively compared to the one obtained by Shao et al. (1998) in their study where they found a fast increase of the bond length follow by a slow increase and a plateau. In the subsequent computations, a position of the instantaneous interfacial point will be plotted as indicated in Figure 5-2a.

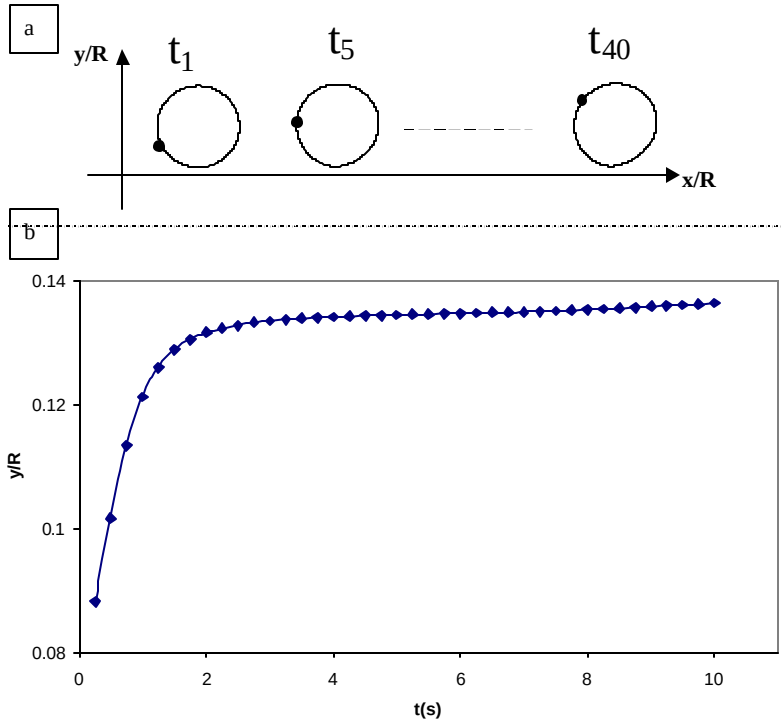

Figure 5-2: Instantaneous position of an interfacial point on the cell for k_{ro} = 1.0 and $\bar{U} = 0.1$, μ = 100, γ = 1.0.

Effect of Bond Molecule

The effect of bond molecules on the behavior of the cell is shown in Figure 5-3. The effect of the wall on the cell displacement is obtained by not activating the micro model (no bond force). It is found that the bond force is strong enough to delay the rolling of the cell and the peeling of the cell from the vessel wall.

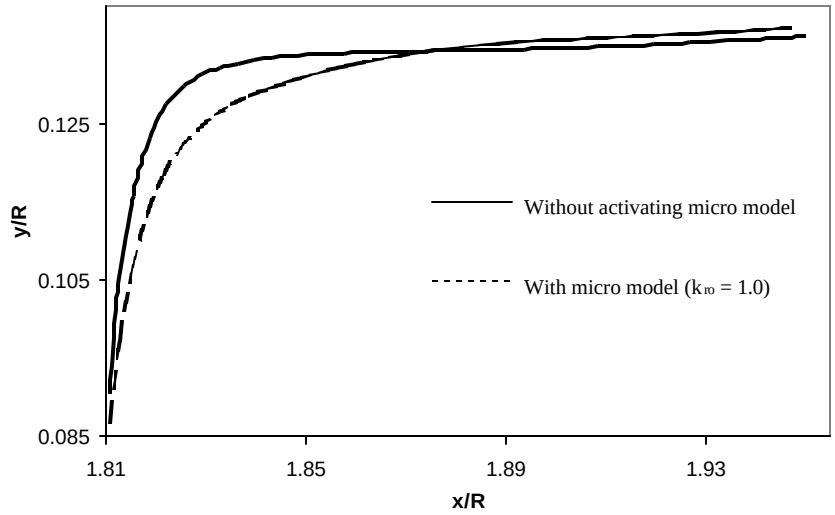

Figure 5-3: Effect of the bond molecules on the rolling of the cell along the wall, $\bar{U} = 0.1$, $\mu = 100$, $\gamma = 1.0$.

Effect of the Reverse Constant k_{ro}

Figure 5-4 shows the effect of the reverse reaction rate k_{ro} on the rolling of the cell. It is observed that an increase in the value of k_{ro} decreases the resistance force from the bond molecules. On the other hand, a lower value of k_{ro} makes the cell rolls for a longer distance, and tends to increase the bond length of the adhesion molecule before breakage as demonstrated by the upper asymptote obtained.

Effect of the Spring Constant

The effect of the spring constant σ on the rolling of the cell is provided in Figure 5-5. Changing the spring constant value by a factor of two has little effect on the rolling

of the cell along the vessel wall. The work by Chang et al. (2000) shows also the little dependence of the spring constant on the adhesion process for some adhesion parameters.

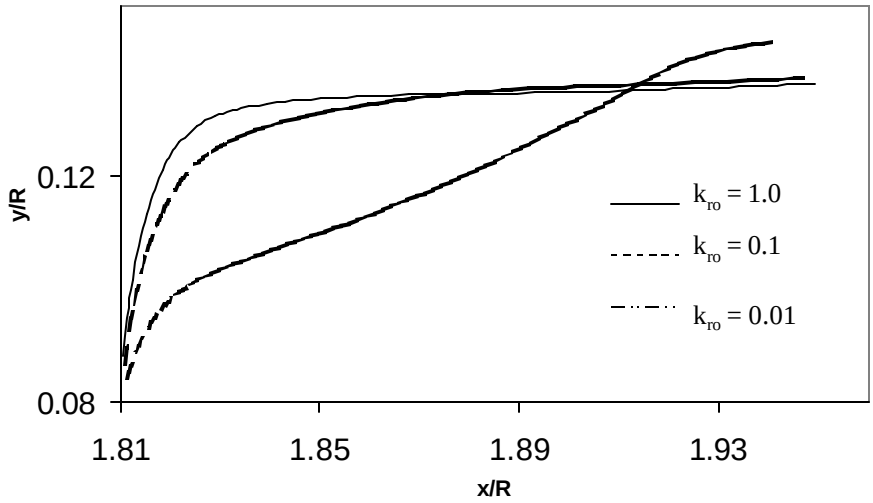

Figure 5-4: Effect of the reverse reaction rate k_{ro} on the rolling of the cell, $\bar{U} = 0.1$, μ = 100, γ = 1.0

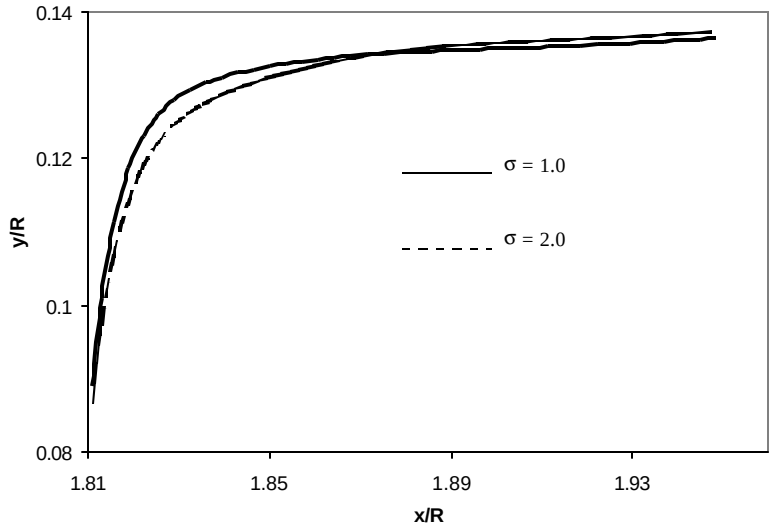

Figure 5-5: Effect of the spring constant on the rolling of the cell. f_s = 0.1, k_{ro} = 1.0, $\bar{U} = 0.1$, μ = 100, γ = 1.0.

Comparison to Existing Results

In the following computations, a bond is considered peeled away from the surface if the cell travels 2 radii. This assumption is based on the shape taken by the cell as a function of time. Kuo et al. (1997) made similar assumptions in their study into which

the leukocyte is modeled as a solid body. They assumed that bonds are broken if the cell travels 10 radii. The best assumption should be based on the adhesion molecule bond strength. The work by Evans (1999) gives a range of adhesion bond strength but not an exact bond strength for a given molecule bond.

Comparison to Numerical Results

Dong et al. (1999) and Dong and Lei 2000) have modeled the cell as a drop enclosed into an elastic ring. In their approach, the initial shape of the elastic ring is the one taken from the picture of an experiment of a cell adhering on a surface subjected to a known shear rate. They assume that only a small portion of the adhesion contact can be peeled away from the wall, but that length is not specified in their work. This assumption allows them to use an energy approach to calculate the cell rolling velocity. In the present model, we do not make that assumption. We solve the full flow field and fluid-interface interactions, and let the flow dictate the contact area. We use the same parameter as in Dong et al. for the adhesion parameters and cell viscosity. The only unknown parameters in their study are the cell surface tension, the contact length and the number of bonds. In the Figure 5-6, a comparison to Dong results is shown for $\bar{g} = 4.0$, 5.0 and 10. The top line corresponds to the higher surface tension, and is in agreement with the results of Dong and Lei (2000). This is expected, since as the surface tension increases, the liquid drop model should provide results similar to the 2D elastic model. However, because our approach is more general, additional information can be found. For example, we do not constraint the cell to a peeling motion only, we allow the cell to be lifted away from the surface.

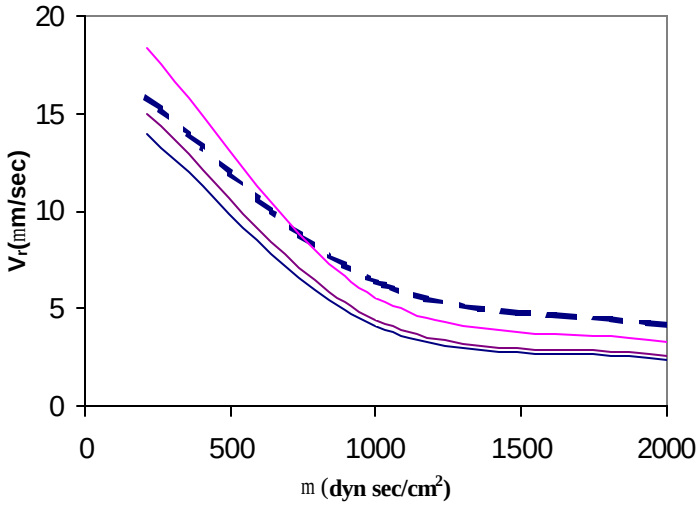

Figure 5-6: Comparison of the cell rolling velocity. The dashed line corresponds to Dong et al. results and the lines to the present study. $\bar{U} = 1.0$, $\bar{N}_r = 0.4$, $\bar{N}_l = 1.06$, $\bar{s} = 0.1$, $f_s = 0.04$, $\bar{g}$ =4.0, 5.0, and 10 from bottom to top respectively.

Comparison to Experimental Results

A comparison of the bond lifetimes computed in this study and the experimental results by Schmidtke and Diamond (2000) for one bond is shown in Figure 5-7. For this comparison, no information about the reaction rates and spring constant exist. But, we have shown that, for the adhesion parameters considered in this study, these values do not significantly affect the rolling and displacement of the cell along the vessel wall. The key parameters are the cell rheological properties, the receptor density and the ligand density. In the present study, we have supposed an excess of ligand number to the number of receptors, the dimensionless cell surface tension is taken to be 1.2 and the dimensionless viscosity ranges from 50 to 300. The top line corresponds to the higher viscosity. Good agreement is seen for the parameters used. An increase in the cell surface tension for a fixed value of cell viscosity will move all the simulated results upward. A surface tension of 1.2 and a viscosity of 200 provide the best fit.

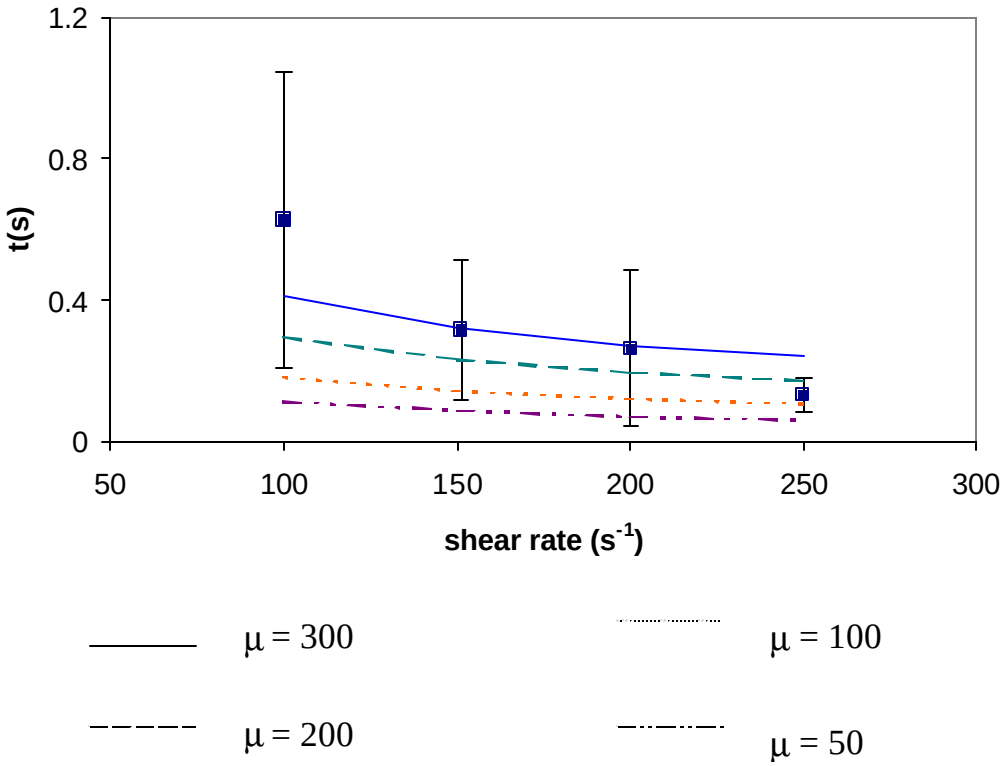

Figure 5-7: Comparison of the bond lifetimes in the simple drop case. The dot corresponds to Schmidtke and Diamond (2000) results and the line to the present study. $\bar{N}_r = 0.02$, $\bar{N}_l = 1.0$, $\bar{s} = 0.1$, $f_s = 0.04$, $\bar{g}$ =1.2.

Compound Drop Model

Figure 5-8 illustrates the problem considered for the compound drop case. Specifically, a nucleated cell is attached to a vessel wall, and a uniform flow is imposed at the inlet of the vessel tube. In the model, the nucleus occupies 44% of the volume of the cell (Schmid-Schonbein et al., 1980), and the rheological properties (viscosity and surface tension) of the nucleus are taken to be 10 times those of the cytoplasm and cellular membrane. The kinetics parameters used are the same as in the simple drop model. The problem to be solved is the same as before: a cell is attached to a vessel wall, with a uniform flow imposed at the inlet of the vessel tube.

It should be noted that the nucleus of a neutrophil is small and segmented. Its contribution may not be as large as the one predicted by the present model but it is difficult to assess this at the present time. A neutrophil nucleus is asymmetric and it has been shown by Kan et al. (1999) that nucleus eccentricity affects the instantaneous shapes of the cell during recovery. In addition, Kan et al. (1998, 1999) have shown that the presence of a nucleus, although small in size, is needed in order to reconcile the various leukocyte rheological data published in the literature. The compound drop model describes better the structure of a lymphocyte, but it is still a good model for evaluating the effect of key parameters on the rheology and adhesion of leukocytes in general.

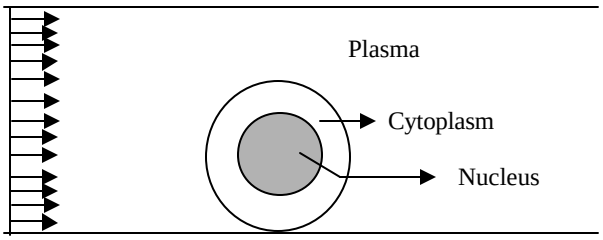

Figure 5-8: Schematic of the problem statement for the compound drop model.

Cell Movement and Deformation

In this paragraph, the displacement and deformation of the cell are studied for different values of cell viscosity, cell surface tension and the inlet boundary condition.

Effect of the Nucleus

Figure 5-9 shows the effect of the nucleus. The nucleus tends to delay the rolling of the cell along the vessel wall but does not appear to affect the bond length before peeling. We also found that the reverse reaction constant within the range studied, $10^{-2} \le k_{ro} \le 10^{-1}$, has no significant effect on the position and displacement of the cell or nucleus. The curves of y/R plotted against t for the compound drop are identical to the one for the liquid drop in Figure 5-2b.

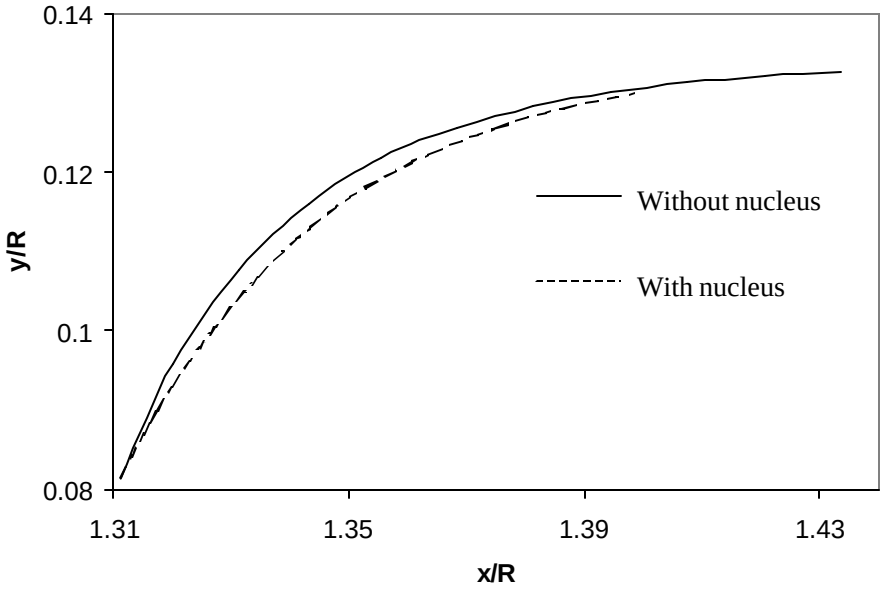

Figure 5-9: Effect of the nucleus on the rolling of the cell along the vessel wall. k_{ro} = 1.0, $\bar{U} = 0.1$, μ = 100, g = 1.0.

Effect of the Viscosity

The effect of viscosity value on the rolling of the cell is investigated for μ = 10 and 100 and is shown in Figure 5-10. A cell with a lower cytoplasmic viscosity deforms more and remains closer to the surface as shown in Figure 5-11.

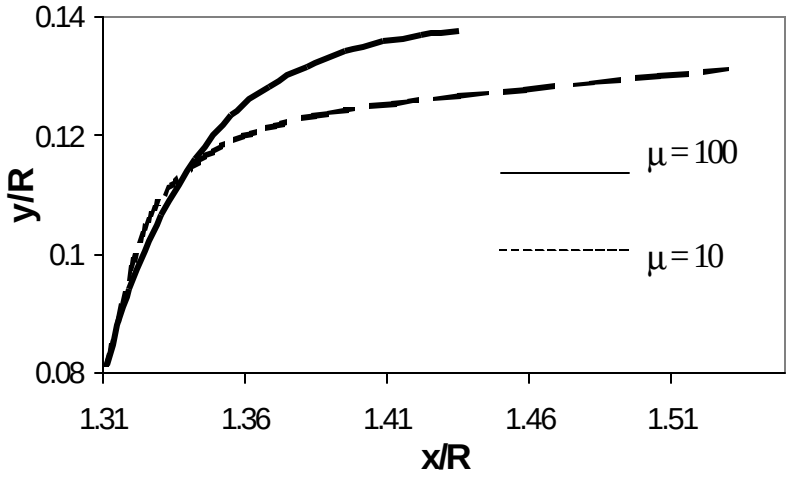

Figure 5-10: Effect of the viscosity on the rolling of the cell along the vessel wall, k_{ro} = 1.0, $\bar{U} = 0.1$, g = 1.0.

Time (t)	μ = 10	μ = 100
0.5	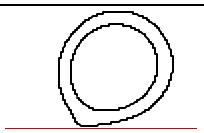	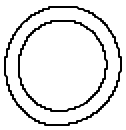
1.0		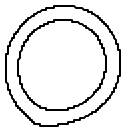
1.5		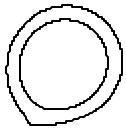

Figure 5-11: Effect of Viscosity on the instantaneous cell Shape. The horizontal line corresponds to the wall.

Effect of the Surface Tension

Surface tension is also found to have a major effect on cell adhesion and rolling as can be seen in Figure 5-12. A lower surface tension allows the cell to maintain a larger curvature, which enable the cell to remain attached with a larger contact area (Figure 5-13). Consequently, a lower surface tension delays the lifting of the cell from the wall.

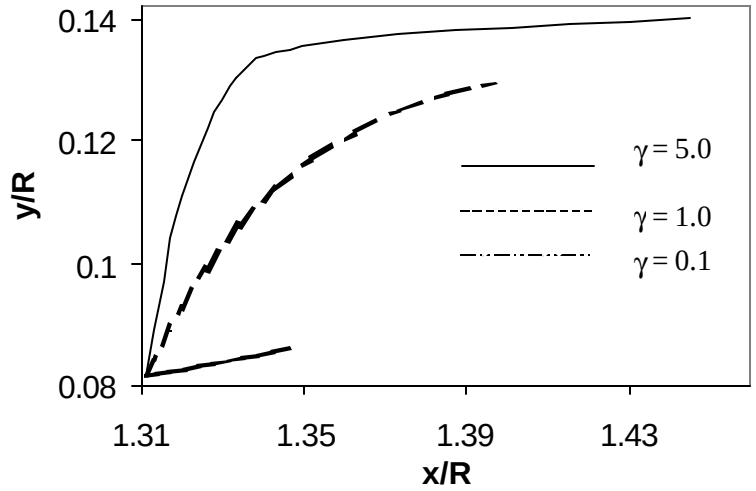

Figure 5-12: Effect of the interfacial tension on the rolling of the cell along the vessel wall, k_{ro} = 1.0, $\bar{U} = 0.1$, μ = 100.

Time (t)	$\gamma = 5$	$\gamma = 1$	$\gamma = 0.1$
1.0	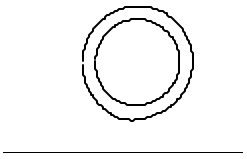	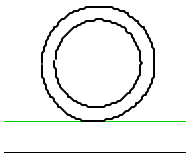	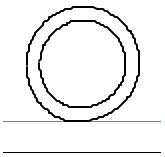
2.0	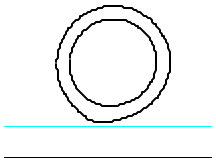	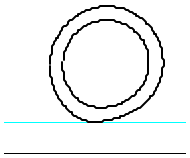	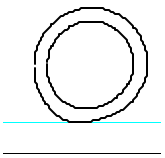
3.0	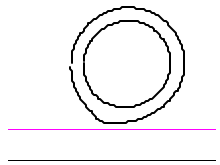	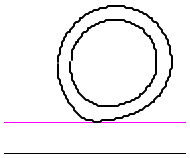	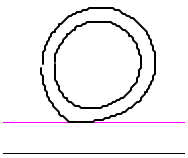
5.0	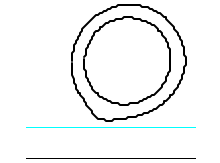	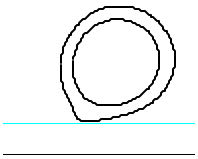	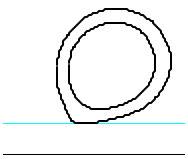

Figure 5-13: Instantaneous cell shape for different values of the interfacial tension. The horizontal line corresponds to the wall.

Effect of the Inlet Boundary Condition

The effect of the inlet velocity is shown in Figure 5-14. As the inlet velocity is increased, the movement of the cell along the vessel wall accelerates and the bond breaks at a shorter distance from the wall. This is due to the fact that when the inlet velocity is increased, the cell is more deformed and stays closer to the wall as shown in Figure 5-15.

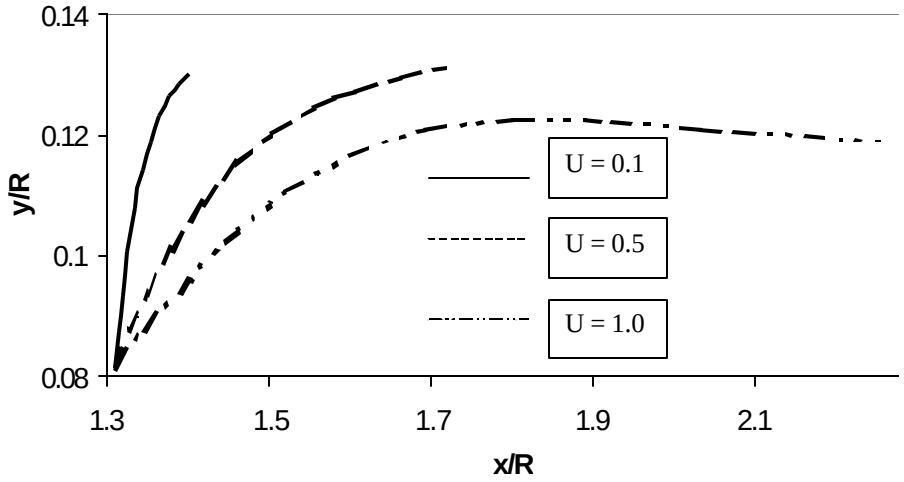

Figure 5-14: Effect of the inlet velocity on the rolling of the cell along the vessel wall, k_{fo} = 1.0, μ = 100, g = 1.0.

Time (t)	U=0.1	U=0.5	U=1.0
1.0			
2.0			
3.0			

Figure 5-15: Instantaneous cell shape for different values of inlet velocities. The horizontal line corresponds to the wall.

Effect of the Capillary Number

Figure 5-16 shows the relative effects of U, μ, and γ on the behavior of the cell for a given capillary number ($Ca=U\mu/\gamma$).

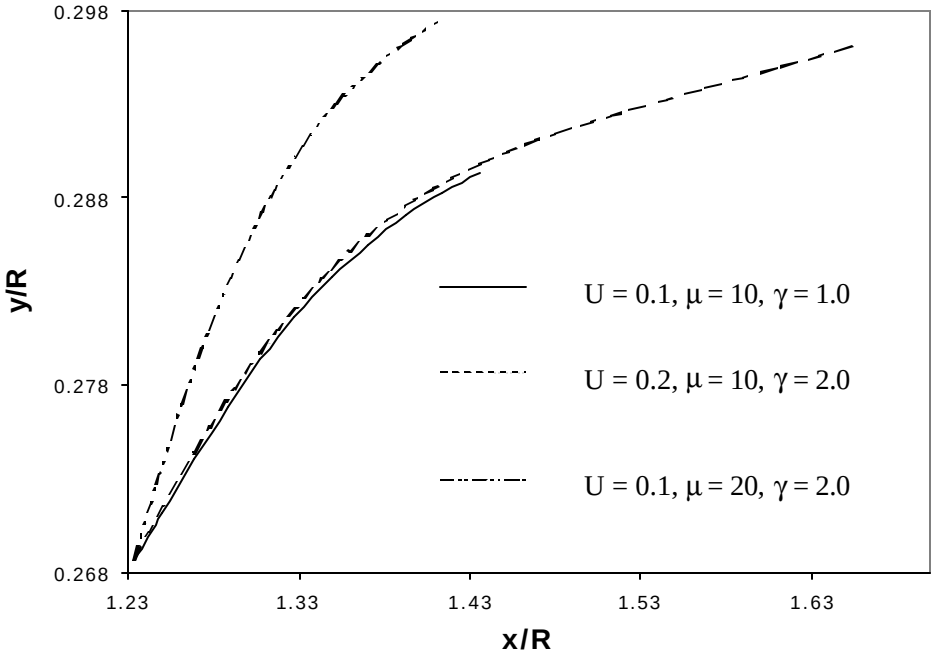

Figure 5-16: Effects of v, μ, and γ for Ca = 10 on the cell behavior, k_{ro} = 1.0

We should point out that when we vary, say, viscosity, other parameters like the viscosity ratio between media, as well as the contribution of the bond force also change. On the other hand, if we hold all other dimensionless parameters the same, and vary Ca, then we will see a unique correlation. This is better understood by looking at the dimensionless form of the equation of motion in the x-direction, for example. By rewriting the equation of motion:

$$r\frac{\partial u}{\partial t} = -\frac{\partial p}{\partial x} + m_i\left(\frac{\partial^2 u}{\partial x^2} + \frac{\partial^2 u}{\partial y^2}\right) + F_g + F_b \tag{32}$$

In dimensionless form using the following reference values, the subscript i refers to the medium of interest:

$$U_{ref} = U_0, \quad p_{ref} = m_0\frac{U_0}{R}, \quad t_0 = \frac{R}{U_0}, \quad F_{gref} = \frac{g}{R^2}, \quad F_{bref} = \frac{s\,l\,N_r}{R} \tag{33}$$

Where U = inlet velocity, R = tube radius, μ_0 = viscosity of the plasma, γ = interfacial tension, σ = spring constant, λ = equilibrium bond length, N_r = receptor density, we obtain:

$$\mathrm{Re}\frac{\partial \bar{u}}{\partial \bar{t}} = -\frac{\partial \bar{p}}{\partial \bar{x}} + a_i\left(\frac{\partial^2 \bar{u}}{\partial \bar{x}^2} + \frac{\partial^2 \bar{u}}{\partial \bar{y}^2}\right) + \frac{1}{Ca}\bar{F}_g + \frac{R l s N_r}{m_0 U_0}\bar{F}_b \tag{34}$$

Where $\alpha_i = \mu_i/\mu_0$ is the viscosity ratio.

Peeling Time and Rolling Velocity Calculation

In what follow, we compute the peeling time, the rolling velocity of a cell adhering to a wall and the force of a bond molecule for different cell properties and adhesion parameters. The following defined parameters will be used for the subsequent computations.

$$a = \frac{m_c}{m_0} \quad and \quad b = \frac{m_n}{m_c} \tag{35}$$

Where μ_0 is the plasma viscosity, μ_c is the cytoplasm viscosity and μ_n is the nucleus viscosity. The reference parameters used are given in Table 5-3 previously listed in the liquid drop model paragraph.

Effect of the Inlet Velocity

Figure 5-17 shows the effect of the inlet velocity flow on the peeling time of the cell from the substratum. An increase of the inlet velocity decreases the peeling time. An inverse relationship can be used to fit the curve as shown in Figure 5-17, and is of the form:

$$\bar{t} = 26.84\bar{U}^{-0.47} \tag{36}$$

where $\bar{t}$ is the dimensionless peeling time and $\bar{U}$ is the inlet velocity flow.

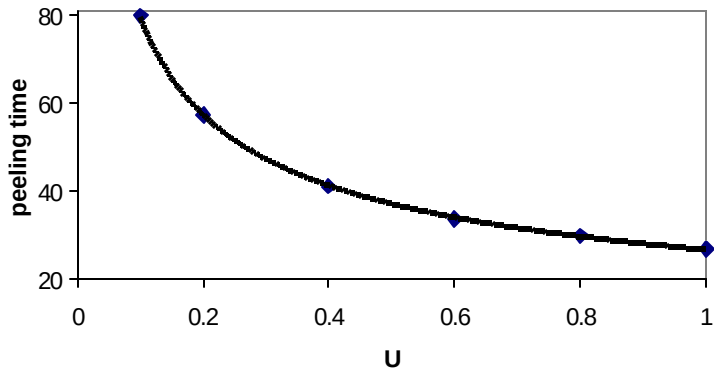

Figure 5-17: Effect of the inlet velocity $\bar{U}$ on the peeling time $\bar{t}$. α = 100, β = 10, $\bar{N}_r = 1.0$, $\bar{N}_l = 1.0$, $\bar{s} = 1.0$, $f_s = 0.2$, $\bar{g} = 1.0$. The dot points correspond to the numerical results and the line is the curve fitting.

Figure 5-18 shows the effect of the inlet velocity flow on the rolling velocity of the leukocyte. The rolling velocity is defined as the ratio of the distance traveled by the cell to the peeling time. Here only the displacement of the cell along the x-axis is shown. An increase of the inlet flow increases the rolling velocity of the cell. The relationship between inlet velocity flow and cell rolling velocity, $\bar{V}_r$, is given by

$$\bar{V}_r = 0.0055\bar{U}^3 - 0.014\bar{U}^2 + 0.017\bar{U} + 0.002. \tag{37}$$

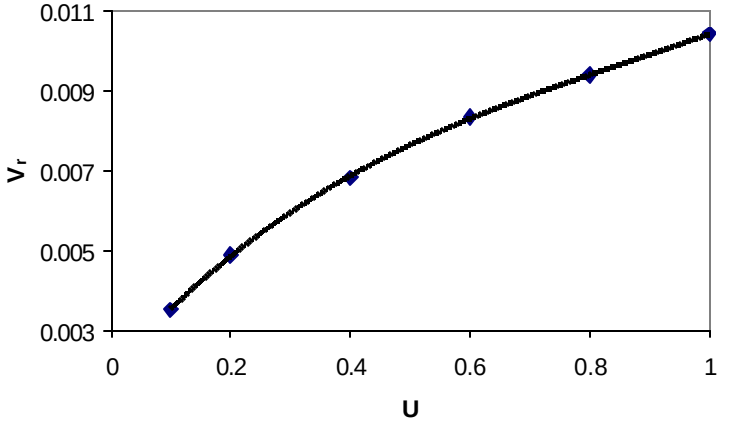

Figure 5-18: Effect of the inlet velocity on the rolling velocity of the leukocyte. α = 100, β = 10, $\bar{N}_r = 1.0$, $\bar{N}_l = 1.0$, $\bar{s} = 1.0$, $f_s = 0.2$, $\bar{g} = 1.0$. The dot points correspond to the numerical results and the line is the curve fitting.

Effect of the Receptor Density

Figure 5-19 and Figure 5-20 show the effects of the receptor density on the peeling time and rolling velocity. An increase of the receptor density increases the peeling time and decreases the rolling velocity. Dong et al. (1999) also found an increase of the peeling time with receptor density. The evolution of the peeling time as a function of the receptor density can be described by the following relationship.

$$\bar{t} = 3.495 Ln(\bar{N}_r) + 76.90 \tag{38}$$

$$\bar{V}_r = 0.0037 \bar{N}_r^{-0.0466} \tag{39}$$

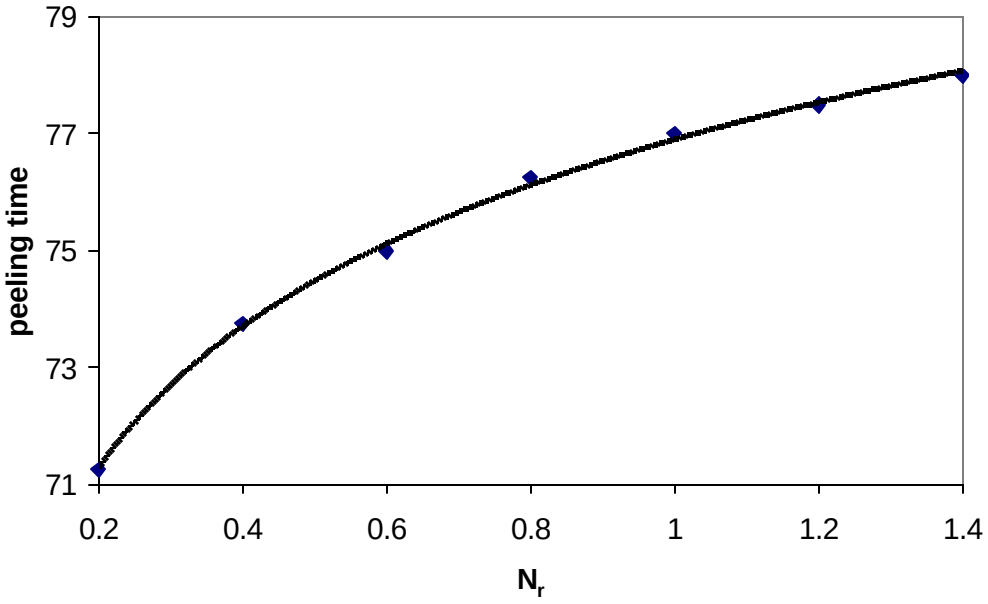

Figure 5-19: Effect of the receptor density $\bar{N}_r$ on the peeling time $\bar{t}$. α = 100, β = 10, $\bar{U} = 0.1$, $\bar{N}_l = 1.0$, $\bar{s} = 1.0$, $f_s = 0.2$, $\bar{g} = 1.0$. The dot points correspond to the numerical results and the line is the curve fitting.

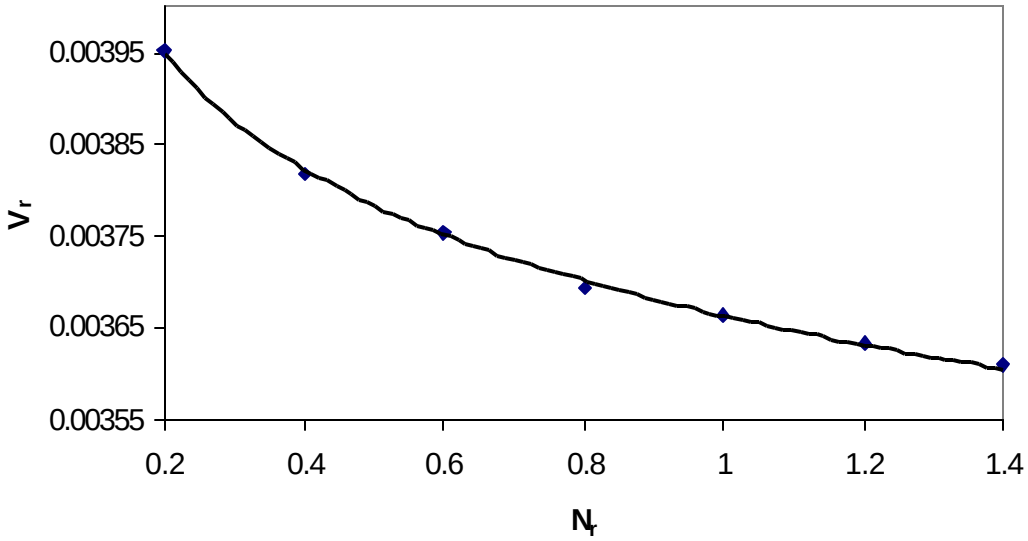

Figure 5-20: Effect of the receptor density $\bar{N}_r$ on the rolling velocity $\bar{V}_r$. α = 100, β = 10, $\bar{U} = 0.1$, $\bar{N}_l = 1.0$, $\bar{s} = 1.0$, $f_s = 0.2$, $\bar{g} = 1.0$. The dot points correspond to the numerical results and the line is the curve fitting.

Effect of the Ligand Density

In Figure 5-21 and Figure 5-22, the effects of ligand density on the peeling time and the rolling are shown. An increase of the ligand density increases the peeling time and decreases the rolling velocity for $\bar{N}_l \leq 1.0$. For $\bar{N}_l >$ 1.0, the peeling time and the rolling velocity remain the same. The following relations are used to describe the dependence:

$$\bar{t} = 2.63 Ln(\bar{N}_l) + 76.91 \tag{40}$$

$$\bar{V}_r = 0.0037 \bar{N}_l^{-0.0352} \tag{41}$$

The plateau is reached because no receptor is available for binding as the ligand density increases. Dong et al. (1999) and Alon et al. (1998) made the same observation in their simulation and experiments respectively.

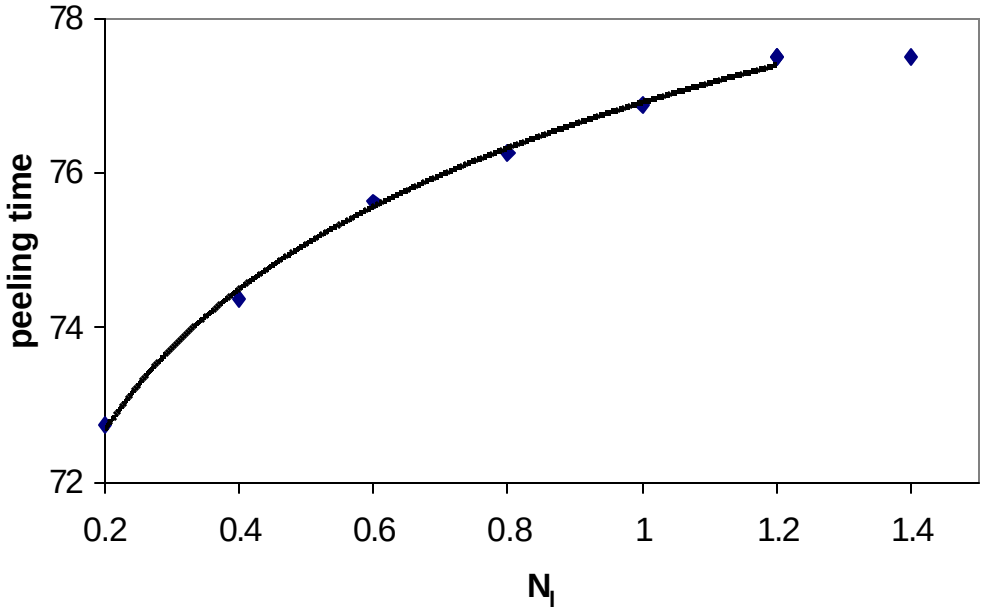

Figure 5-21: Effect of the ligand density $\bar{N}_l$ on the peeling time $\bar{t}$. α = 100, β = 10, $\bar{U} = 0.1$, $\bar{N}_r = 1.0$, $\bar{s} = 1.0$, $f_s = 0.2$, $\bar{g} = 1.0$. The dot points correspond to the numerical results and the line is the curve fitting.

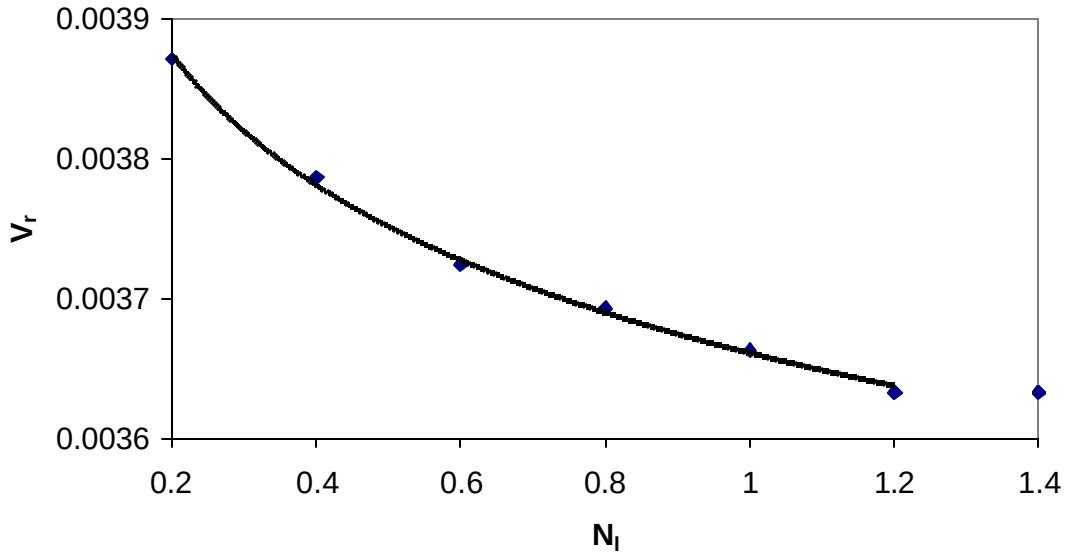

Figure 5-22: Effect of the ligand density $\bar{N}_l$ on the rolling velocity $\bar{V}_r$. α = 100, β = 10, $\bar{U} = 0.1$, $\bar{N}_r = 1.0$, $\bar{s} = 1.0$, $f_s = 0.2$, $\bar{g} = 1.0$. The dot points correspond to the numerical results and the line is the curve fitting.

Effect of the Surface Tension

The effect of the surface tension on the peeling time shows an inverse dependence as observed in Figure 5-23.

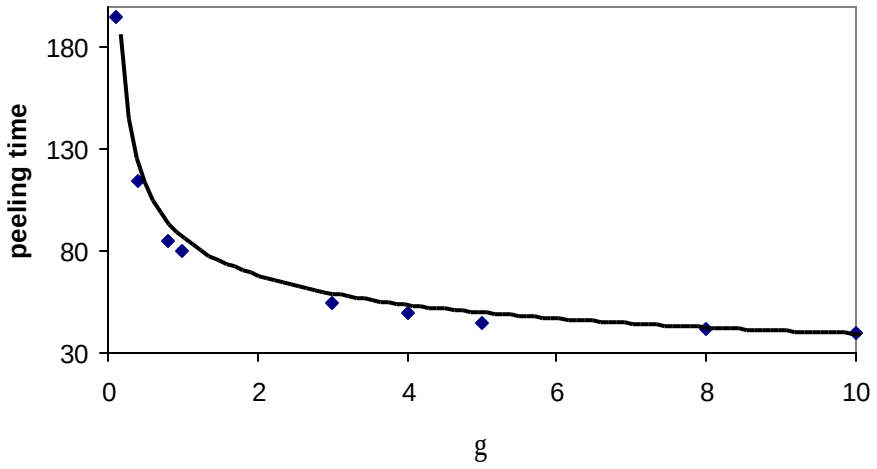

Figure 5-23: Effect of the surface tension on the peeling time $\bar{t}$. α = 100, $\bar{U} = 0.1$, $\bar{N}_r = 1.0$, $\bar{N}_l = 1.0$, $\bar{s} = 1.0$, $f_s = 0.2$, $b = 10$. The dot points correspond to the numerical results and the line is the curve fitting.

The following relation can be used to describe this dependence

$$\bar{t} = 82.78\bar{g}^{-0.3483}. \tag{42}$$

In addition, an increase of the surface tension increases the rolling velocity as shown in Figure 5-24.

For $\bar{g} \le 1.0$, the relationship can be described by

$$\bar{V}_r = -0.0018\bar{g}^{-2} + 0.0043\bar{g} + 0.001, \tag{43}$$

while for $\bar{g} \ge 1.0$, the relation is given by

$$\bar{V}_r = 5.10^{-6}\bar{g}^{-3} - 10^{-4}\bar{g}^{-2} + 0.0013\bar{g} + 0.0023 \tag{44}$$

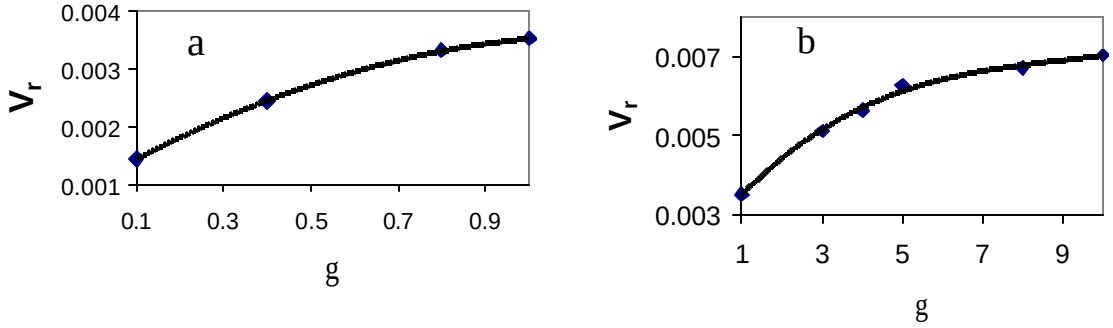

Figure 5-24: Effect of the surface tension on the rolling velocity $\bar{V}_r$. α = 100, $\bar{U} = 0.1$, $\bar{N}_r = 1.0$, $\bar{N}_l = 1.0$, $\bar{s} = 1.0$, $f_s = 0.2$, $b = 10$, $\bar{g} \le 1.0$ (a) and $\bar{g} \ge 1.0$ (b). The dot points correspond to the numerical results and the line is the curve fitting.

Effect of the Parameter β

Figure 5-25 and Figure 5-26 show the effect of the parameter β, which is the ratio of the nucleus viscosity to the cytoplasm viscosity, on the peeling time and rolling velocity. An increase of β increases the peeling time and decreases the rolling velocity. A third order polynomial can be used to fit the computational points.

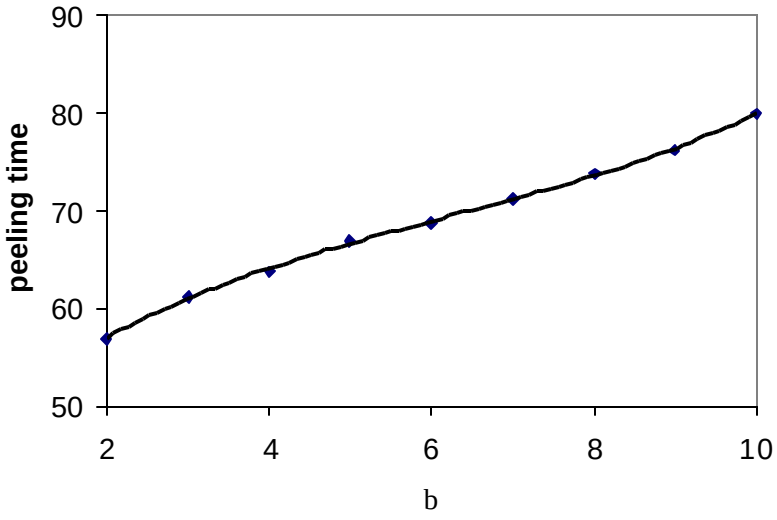

Figure 5-25: Effect of β on the peeling time. α = 100, $\bar{U} = 0.1$, $\bar{N}_r = 1.0$, $\bar{N}_l = 1.0$, $\bar{s} = 1.0$, $f_s = 0.2$. The dot points correspond to the numerical results and the line is the curve fitting.

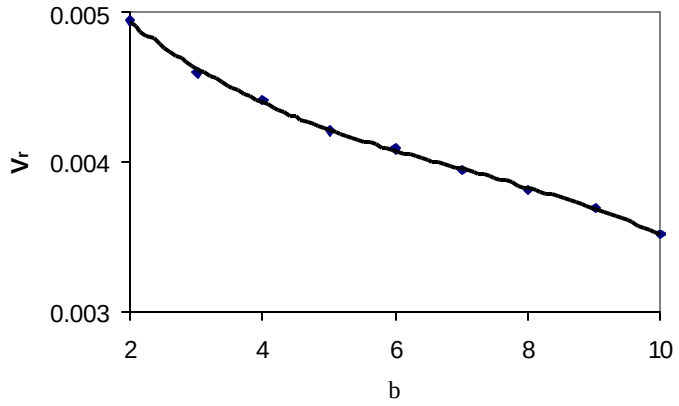

Figure 5-26: Effect of β on the rolling velocity. α = 100, $\bar{U} = 0.1$, $\bar{N}_r = 1.0$, $\bar{N}_l = 1.0$, $\bar{s} = 1.0$, $f_s = 0.2$. The dot points correspond to the numerical results and the line is the curve fitting.

Effect of the Parameter α

The effects of the parameter α, defined as the ratio of the cytoplasm viscosity to the plasma viscosity, on the peeling time and rolling velocity are illustrated in Figures 5-27 and 5-28 respectively. An increase of α slows the breakage of the formed bonds and the cell rolling velocity. A third order polynomial and an inverse power are found to best fit the responses of the peeling time and the velocity, respectively.

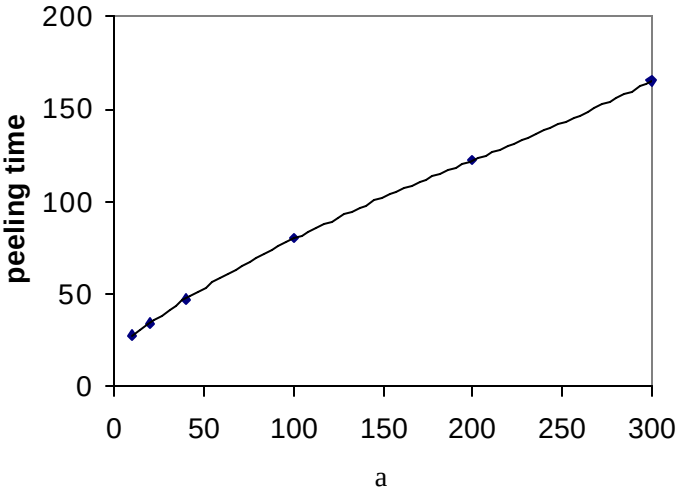

Figure 5-27: Effect of α on peeling time. β = 10, $\bar{U} = 0.1$, $\bar{N}_r = 1.0$, $\bar{N}_l = 1.0$, $\bar{s} = 1.0$, $f_s = 0.2$. The dot points correspond to the numerical results and the line is the curve fitting.

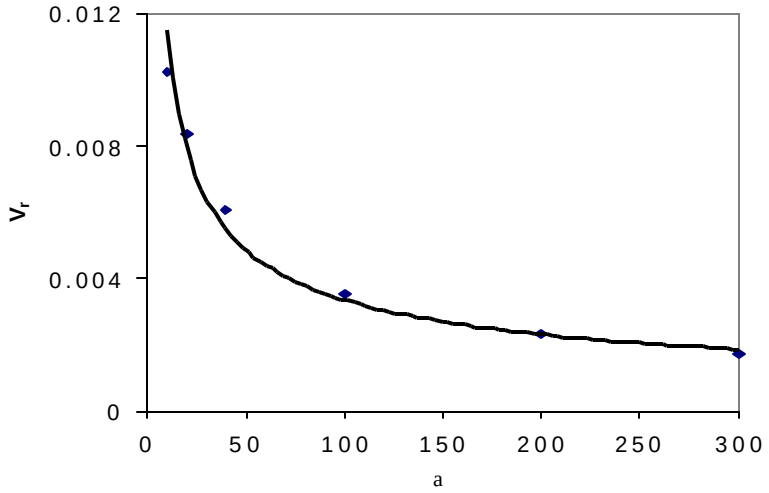

Figure 5-28: Effect of α on the rolling velocity. β = 10, $\bar{U} = 0.1$, $\bar{N}_r = 1.0$, $\bar{N}_l = 1.0$, $\bar{s} = 1.0$, $f_s = 0.2$. The dot points correspond to the numerical results and the line is the curve fitting.

Effect of the Contact Length

The effect of the initial contact length was also investigated in this study. An increase of the contact length augments the initial bond number as indicated by Equation (45):

$$n_b = 1.4q + 7 \tag{45}$$

where n_b is the number of bonds and θ is defined in Figure 5-29.

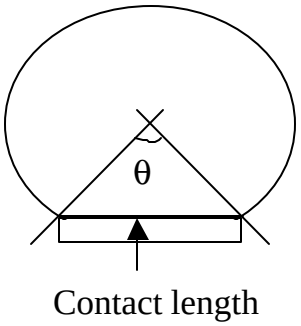

Figure 5-29: Angle and contact length definitions

In addition, an increase of the contact length rises the peeling time and reduces the cell rolling velocity as shown in Figures 5-30 and 5-31, respectively. The

relationships between the initial contact length, the peeling time and the velocity are given by:

$$\bar{t} = 0.0125q^2 + 0.825q + 67.813 \tag{46}$$

$$\bar{V}_r = -4.10^{-5}q + 0.0041 \tag{47}$$

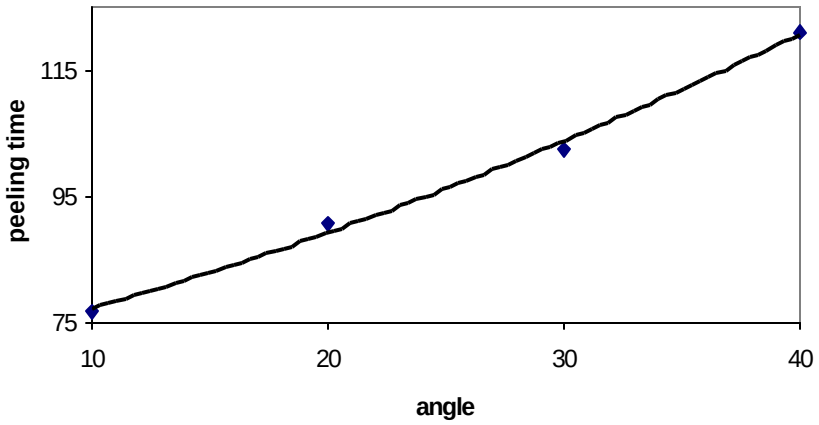

Figure 5-30: Effect of the contact length on the peeling time $\bar{t}$. α = 100, $\bar{U} = 0.1$, $\bar{N}_r = 1.0$, $\bar{N}_l = 1.0$, $\bar{s} = 1.0$, $f_s = 0.2$, $b = 10$, $\bar{g} = 1.0$. The dot points correspond to the numerical results and the line is the curve fitting.

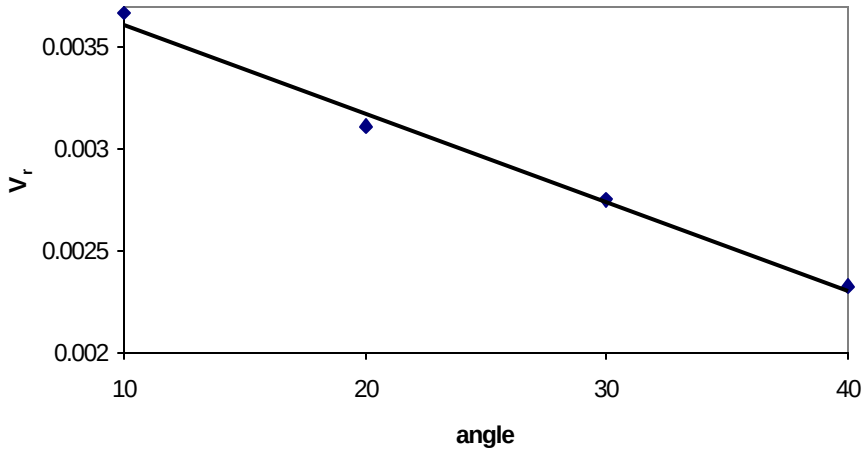

Figure 5-31: Effect of the surface tension on the rolling velocity $\bar{V}_r$. α = 100, $\bar{U} = 0.1$, $\bar{N}_r = 1.0$, $\bar{N}_l = 1.0$, $\bar{s} = 1.0$, $f_s = 0.2$, $b = 10$. The dot points correspond to the numerical results and the line is the curve fitting.

Comparison to Experimental Results

A comparison of our results to the experimental results obtained by Schmidtke and Diamond (2000) is conducted by first fixing the cell surface tension and varying the cell viscosity and then the cell viscosity is held fixed while varying cell surface tension. In this computation, the number of bonds is taken to be small.

Effect of Cell Viscosity on Bond Lifetime

Comparisons between the experimental data by Schmidtke and Diamond (2000) and the compound drop model results of N'Dri et al. (2002) are shown in Figure 5-32, for viscosity values of 50, 100 200 and cytoplasmic viscosity to nucleus viscosity ratios of 5 and 10. The interfacial tension is fixed at 1.2. The lifetime of the bonds decreases with the amount of applied shear rate, and if the cell cytoplasm is less viscous. Within the standard deviations of the experimental data, the compound drop model with a cytoplasmic viscosity equals to 50 fits the data. However, the model with a cytoplasmic viscosity of 100 describes better the experimental data for shear rates up to 250 s^{-1}. It is also seen that if the nucleus is more viscous, it will increase the lifetime of the bonds.

Effect of Cell Surface Tension on Bond Lifetime

As shown in Figure 5-33, fixing the cell viscosity and varying the surface tension allows us to assess the surface tension effect on the bond lifetime. Higher surface tension shows agreement with the experimental results obtained by Schmidtke and Diamond (2000). Again an increase of surface tension decreases the bond lifetime.

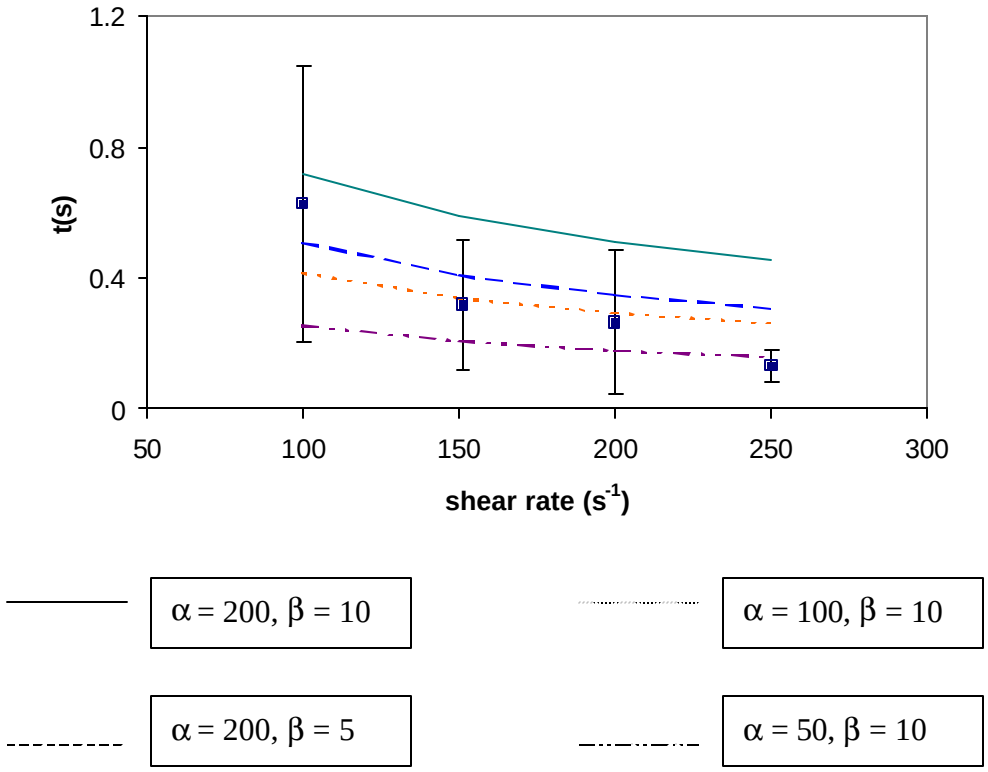

Figure 5-32: Comparison of the bond lifetimes for the compound drop case. The dot corresponds to Schmidtke and Diamond (2000) results and the lines to N'Dri et al. (2002). $\bar{N}_r = 0.02$, $\bar{N}_l = 1.0$, $\bar{s} = 0.1$, $f_s = 0.04$, $\bar{g}$ =1.2.

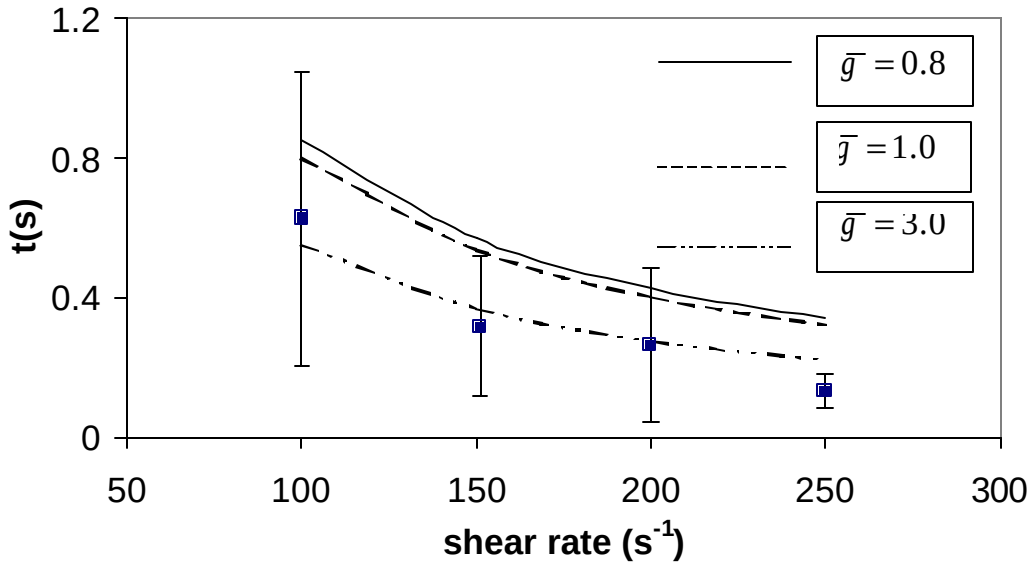

Figure 5-33: Effects of surface tension and shear rate on the bond lifetime: compound drop model. The dot corresponds to Schmidtke and Diamond (2000) results and the lines to the present study. $\bar{N}_r = 1.0$, $\bar{N}_l = 1.0$, $\bar{s} = 0.1$, $f_s = 0.04$, α = 100 and β = 10.

Effect of Applied Hydrodynamic Force on the Bond Lifetime

The bond lifetime is shown as a function of the applied hydrodynamic force for a cytoplasmic viscosity equal to 200 in Figure 5-34. An exponential function, as proposed by Shao and Hochmuth (1999), can be used to describe the results as indicated in Figure 4-34a.

The hydrodynamic force is computed as follows

$$F = mUd \tag{48}$$

where μ is the plasma viscosity, U the inlet velocity and d the tube diameter.

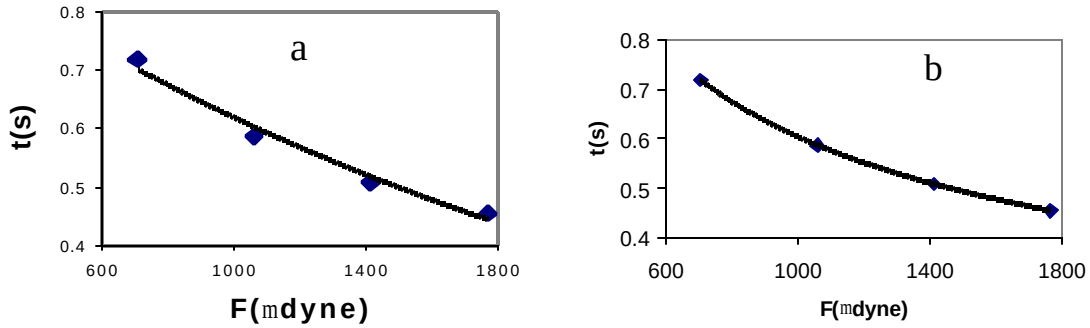

Figure 5-34: Bond lifetimes as a function of applied force. $\bar{N}_r = 0.02$, $\bar{N}_l = 1.0$, $\bar{s} = 0.1$, $f_s = 0.04$, $\bar{g}$ =1.2, $b = 10$, α = 200. The dot points correspond to the numerical results and the line is the curve fitting, (a) exponential fit; (b) inverse power fit.

The exponential relationship,

$$t = 0.95\mathrm{e}^{-0.0004F}, \tag{49}$$

provides a good fit to the data, however, an inverse correlation between the applied force or pulling force and the bond lifetime, gives the best fit to the data (Figure 5-34b). An increase of the pulling force decreases the bond lifetime as observed by many authors (Evans, 1999; Smith and Lawrence, 1999).

$$t = \frac{19.1}{\sqrt{F}}, \tag{50}$$

Bond Rupture Force F_{br}

The force of rupture of a single bond, F_{br}, was also determined. This force is the force reaches by the bond before it breaks. The critical bond forces computed by Goldman et al. (1967b) and Dong et al. (1999) are reported to be between 100 and 400 pN and 100 and 200 pN, respectively. In the literature, experimental measurements give forces of rupture between 37 and 250 pN (Shao and Hochmuth, 1996; Smith and Lawrence, 1999). Evans (1999) found bond strength of 200-300 pN for biotin-streptavidin and a value of bond strength of order 160pN for biotin-avidin. In the work of N'Dri et al. (2002), the values of the bond molecule force vary from 250 to 400 pN for a range of shear flows between 2 and 20 dyne/cm^2 and a spring constant $\bar{s} = 0.1$. These results are shown in Figure 5-35 for α = 100. The value of $\bar{s} = 0.1$ corresponds to a dimensional value of 0.5 dyne/cm as used in the computation of Dong and Lei (2000). Lower values of F_{br} can be obtained by decreasing the value of the spring constant. A lower force of rupture means a shorter bond lifetime. Figure 5-35 demonstrates a linear relationship between bond lifetime and force of rupture,

$$t = 0.0013F_{br} - 0.206 \tag{51}$$

N'Dri et al. (2002) found that using a bond stiffness $\bar{s} \leq 0.06$ (σ = 0.3 dyn/cm) gives the range of bond forces reported in the literature. It is important to note that Shao and Hochmuth (1996) have reported a spring constant value of 43pN/μm (0.043 dyne/cm), which is much smaller than the values cited above. Using the range of force computed in this study, the length reached by a bond before breakage was computed and is found to lie between 0.25 and 0.85 μm. The measured bond length found in the literature is between 0.1 and 0.7 μm (Shao et al., 1998).

Effect of Viscosity on Bond Rupture Force

The bond lifetime as a function of the shear for different values of the viscosity was shown in Figure 5-33. Using equation (51), one can assess the effect of viscosity on rupture force of a bond for a fixed value of the inlet boundary condition. The result is shown in Figure 5-36. An increase of the viscosity for a fixed applied hydrodynamic force increases linearly with the rupture force.

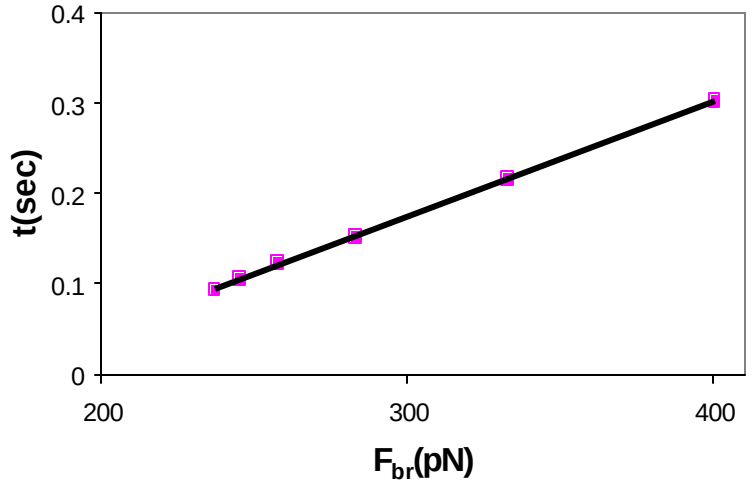

Figure 5-35: Bond lifetime t as a function of bond force F_{br}. $\bar{N}_r = 0.02$, $\bar{N}_l = 1.0$, $\bar{s} = 0.1$, $f_s = 0.04$, $\bar{g}$ =1.2, $b = 10$. The dot points correspond to the numerical results and the line is a curve fitting.

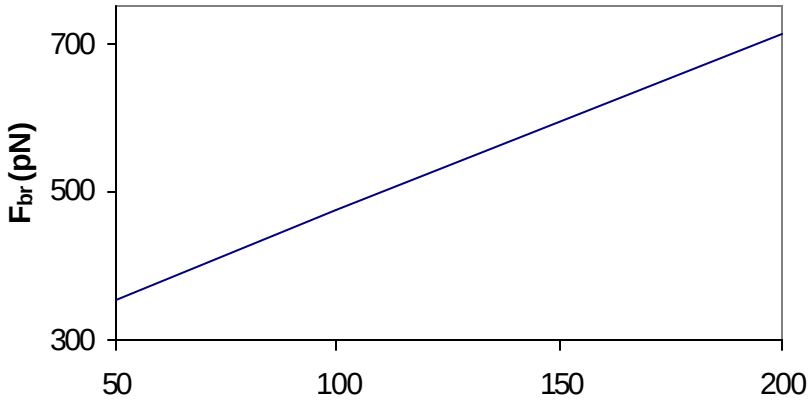

a

Figure 5-36: Effect of the viscosity on the bond rupture force. $\bar{N}_r = 0.02$, $\bar{N}_l = 1.0$, $\bar{s} = 0.1$, $f_s = 0.04$, $\bar{g}$ =1.2, $b = 10$.

Effect of Interfacial Tension on Bond Rupture Force

Using Figure 5-34 and Equation (51), we can assess the effect of the surface tension on the bond rupture force. An increase of the surface tension inversely decreases with the bond rupture force for a fixed applied hydrodynamic force as shown in Figure 5-37.

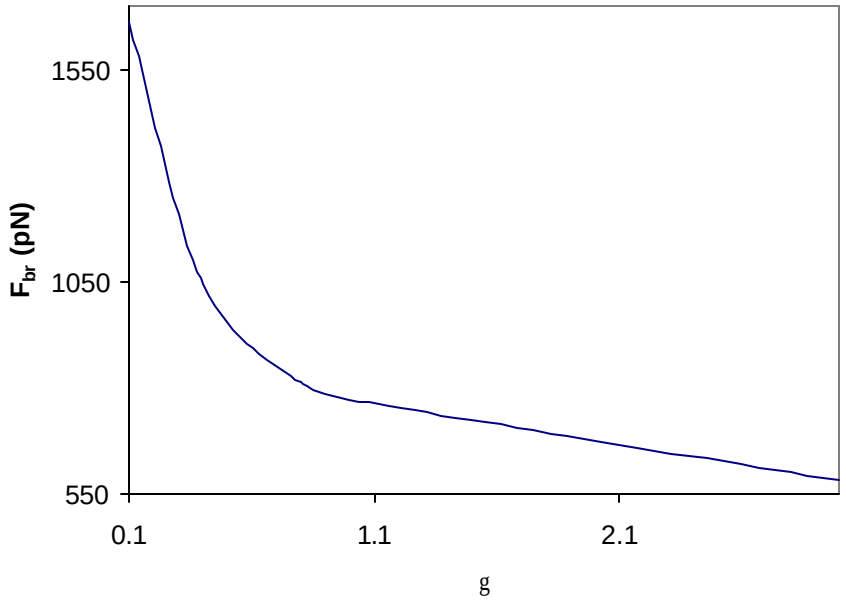

Figure 5-37: Effect of the surface tension on the bond rupture force. $\bar{N}_r = 0.02$, $\bar{N}_l = 1.0$, $\bar{s} = 0.1$, $f_s = 0.04$, $b = 10$, α=100.

Multiple Bond Case

Finally, the case of multiple bonds is shown in Figure 5-38. In Schmidtke and Diamond (2000), only a shear rate of 150 s^{-1} was studied. In the present computation, as in the case of a single bond, shear rates vary between 100 and 250 s^{-1}, the cytoplasmic viscosity is 100, and the interfacial tension ranges from 0.1 to 3.0. The number of bonds is not known in the work of Schmidtke and Diamond (2000), but in the simulation of N'Dri et al. (2002) the bond number is 7. The bond lifetime is higher for a cell with a lower surface tension. The top curve corresponds to the cell with the lowest surface

tension. In addition, an increase of bonds or cell viscosity will extend the bond lifetime as suggested in Figures 5-19, 5-25, 5-27.

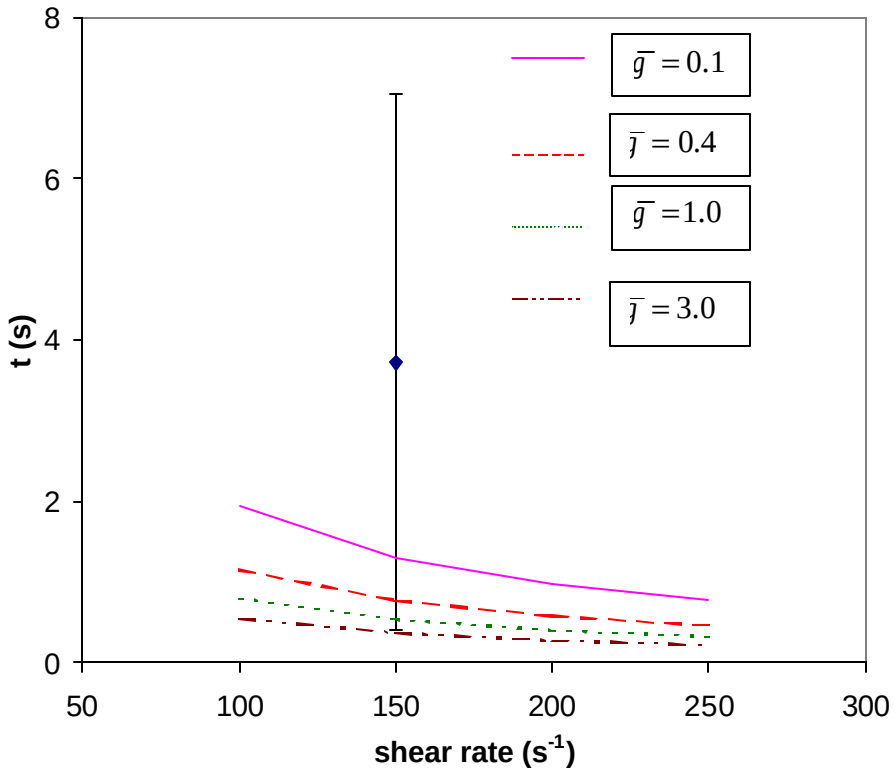

Figure 5-38: Comparison of the computed bond lifetimes in the case of compound drop and multiple bonds. The dot corresponds to Schmidtke and Diamond (2000) results and the line to N'Dri et al. (2002). $a = 100$, $\bar{N}_r = 1.0$, $\bar{N}_l = 1.0$, $\bar{s} = 1.0$, $f_s = 0.04$, $b = 10$.

In summary, from the work of N'Dri et al. (2002) using the multi-scale approach outlined in chapter 4, it is shown that cell deformability affects the rolling of a cell along a vessel wall. A cell with a higher surface tension rolls faster. These results are in agreement with those of Dong and Lei (2000) where only a small section of the membrane is allowed to deform. The results also show that as the shear rate increases, the bond lifetime decreases as observed by Schmidtke and Diamond (2000). The bond lifetime is also found to increase as the cell or nucleus viscosities increase.

Effect of the Cell Diameter

There are three types of leukocytes with different diameters, the lymphocytes with 7μm, the neutrophils with 8μm, and the monocytes with 10μm in diameter in average. The effect of different cell diameters for a fixed tube diameter on the peeling time is shown in Figure 5-39. A larger cell diameter decreases the peeling time and increases the cell rolling velocity as shown in Tran-Son-Tay et al. (2002). This result is consistent with the simulation and experimental results found by Tees et al. (2002) and by Patil et al. (2001), respectively. A larger cell causes a higher blockage in the tube, which results in larger hydrodynamic forces. Considering that the velocity scales inversely and linearly with the tube opening (and hence scales linearly with the cell size) to satisfy mass continuity, and the pressure force scales quadratically with the velocity, the hydrodynamic force on the cell increases more than linearly with the cell diameter.

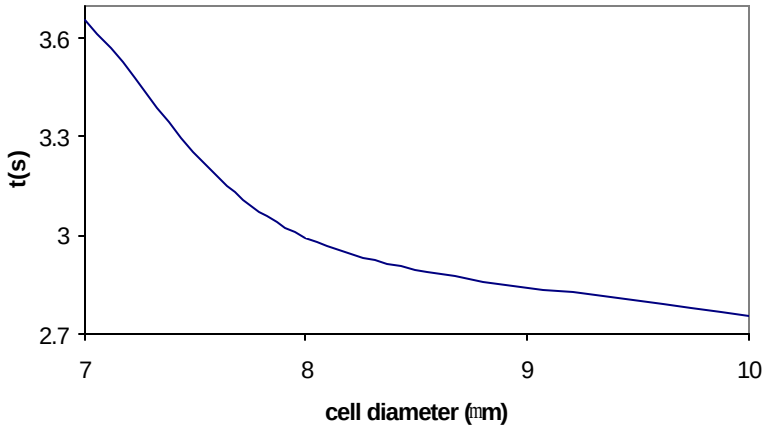

Figure 5-39: Effect of cell diameter on the peeling time of the cell. α = 100, $\bar{U} = 0.1$, $\bar{N}_r = 1.0$, $\bar{N}_l = 1.0$, $\bar{s} = 1.0$, $f_s = 0.2$, $b = 5$.

Effect of the Vessel Diameter

The blood vessel diameter varies from centimeter to micrometer in the circulatory system, in order to study the effect of the vessel diameter on cell adhesion, we compute

the peeling time of an adherent cell for three different diameters. Figure 5-40 shows the result of such a computation, where we found that an increase of the vessel diameter decreases the peeling time and increases the cell rolling velocity. Increasing the vessel diameter increases the applied hydrodynamic force.

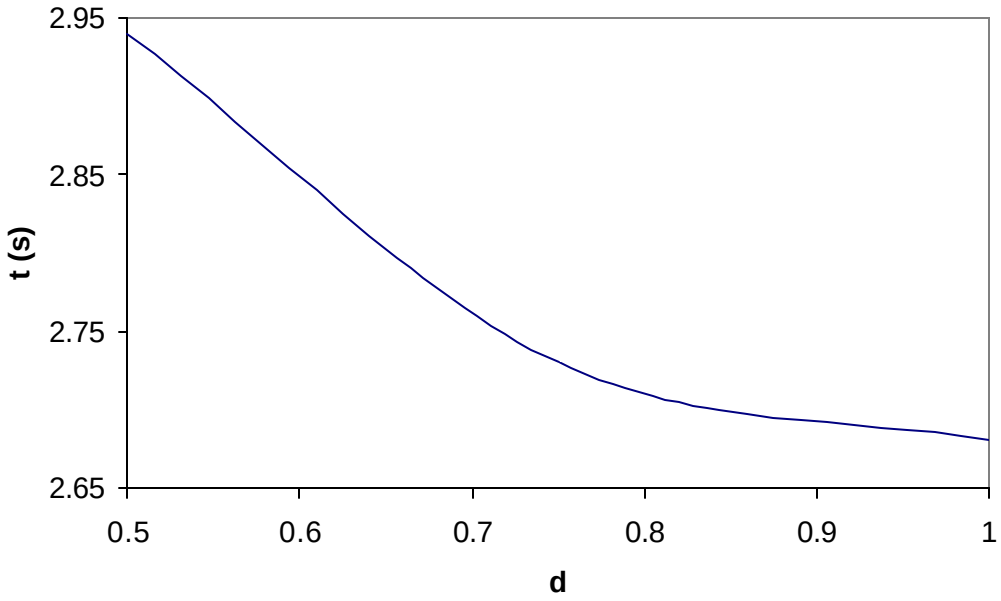

Figure 5-40: Effect of vessel diameter on the peeling time of the cell. α = 100, $\bar{U} = 0.1$, $\bar{N}_r = 1.0$, $\bar{N}_l = 1.0$, $\bar{s} = 1.0$, $f_s = 0.2$, $b = 5$.

Effect of the Pulsatile Inlet Boundary Condition

The effect of the inlet pulsatile boundary condition on the peeling of the cell is also assessed. Equation (52) shows the boundary condition used and Figure 5-41 shows the number of pulses studies in the present work.

$$U_P(t) = \frac{1}{10}\sum_{n=1}^{4} \sin(np\,t) \qquad (52)$$

Where U_P is the inlet velocity and t the time.

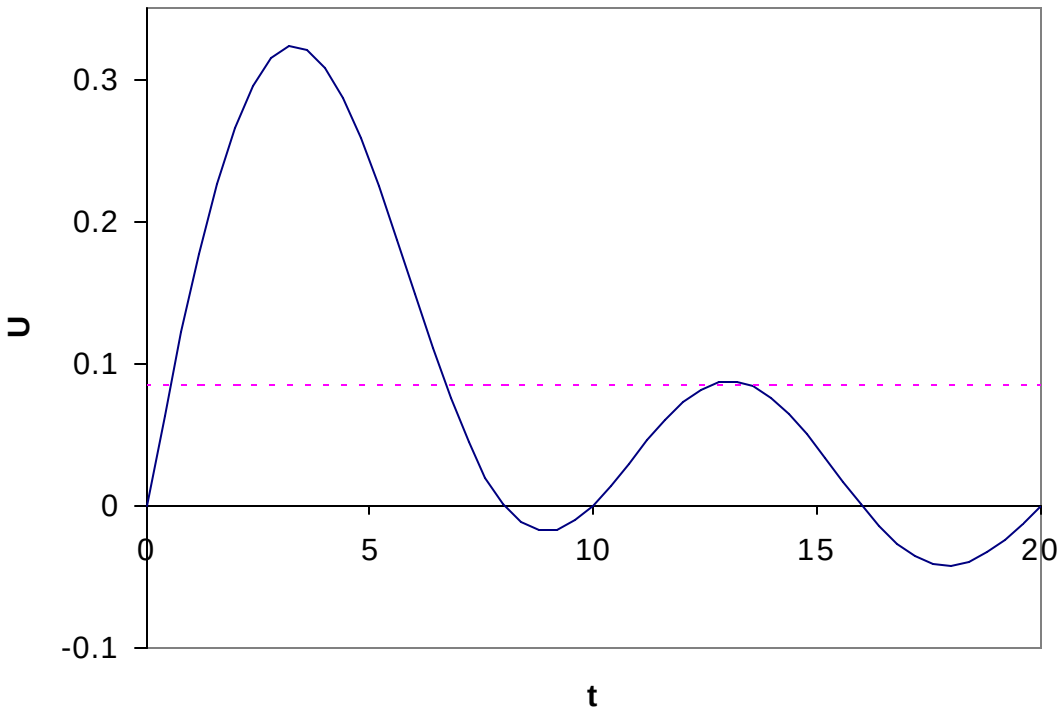

Figure 5-41: Pulsatile (line) and uniform (dashed line) inlet boundary conditions used in the present work.

Comparison of the Peeling Time for the Uniform and Pulsatile Conditions

Figure 5-42 shows a comparison of the pulsatile and uniform inlet boundary conditions for different values of the surface tension. The uniform boundary condition is computed by taking the average of the pulsatile velocity over one period.

$$U = \frac{1}{T}\int_0^T U_P(t)\,dt \tag{53}$$

where T is the time period.

We observed that the peeling time is higher for the uniform inlet velocity than that of the pulsatile boundary condition.

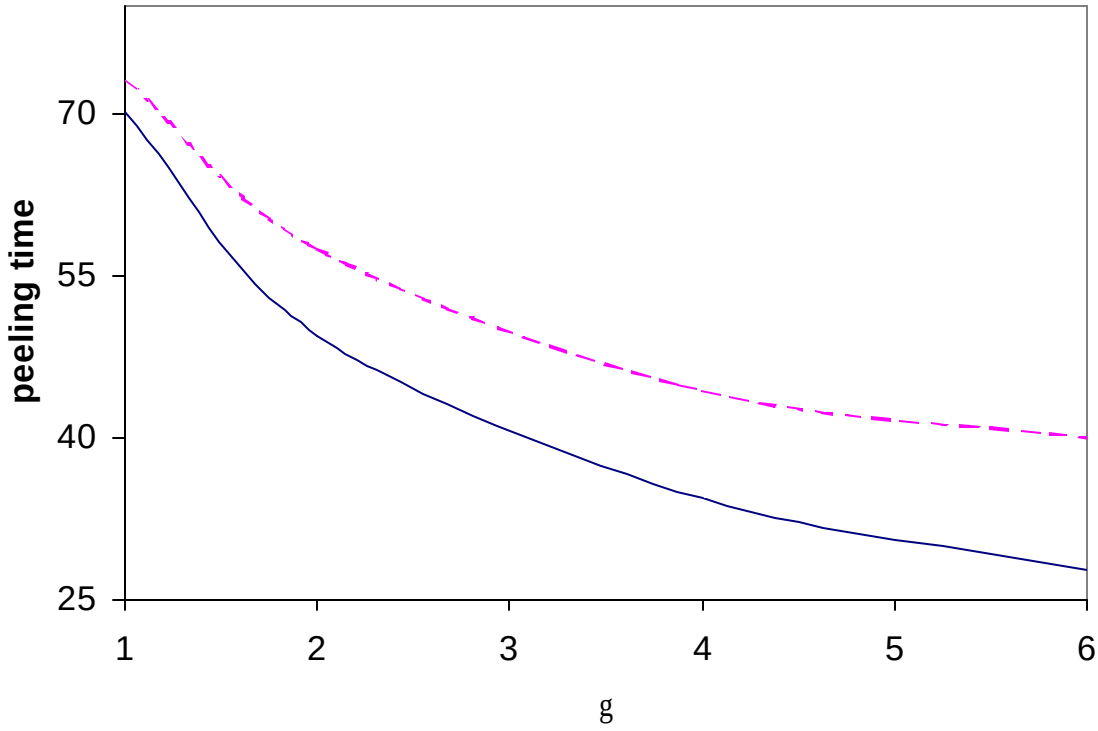

Figure 5-42: Comparison of peeling time for the pulsatile (line) and uniform (dashed line) inlet boundary condition for different values of the surface tension. α = 100, $\bar{N}_r = 1.0$, $\bar{N}_l = 1.0$, $\bar{s} = 1.0$, $f_s = 0.2$, $b = 10$.

Effect of the Surface Tension on the Pulse Number

Figure 5-43 shows the effect of the cell surface tension on the number of pulses needed to peel the cell away from the wall. An increase of the surface tension decreases the number of pulses.

The approximate curve that can be used to fit the experimental points is given below:

$$n_p = -0.82\ln(\bar{g}) + 2.08 \qquad (54)$$

where n_p is the number of pulses

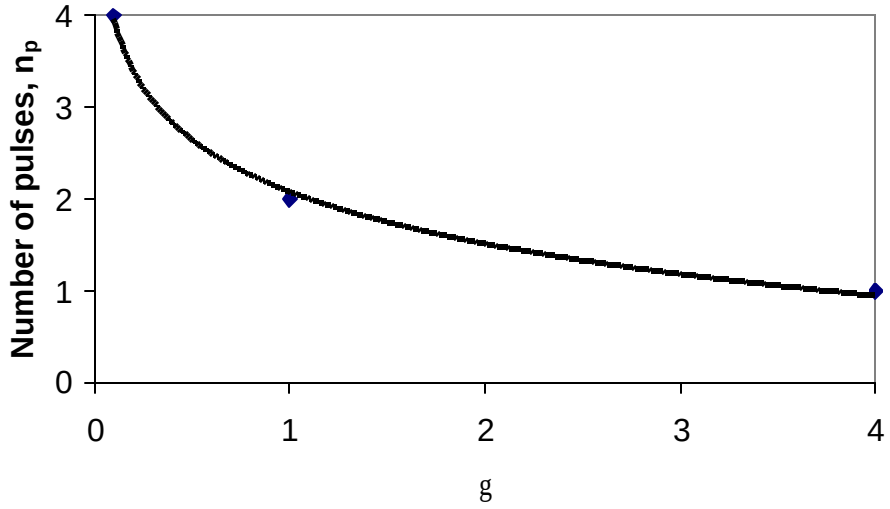

Figure 5-43: Effect of the cell surface tension on the number of pulses n_p. α = 100, $\bar{N}_r = 1.0$, $\bar{N}_l = 1.0$, $\bar{s} = 1.0$, $f_s = 0.2$, $b = 10$. The dot corresponds to the numerical results and the line is the curve fitting.

Effect of the Parameter α on the Pulse Number

The study of the effect of the parameter β, ratio of the nucleus viscosity to the cytoplasmic viscosity, has shown no difference for the range $(1 \le b \le 10)$ used in the present study. On the other hand, the effect of the parameter α, ratio of the cytoplasmic viscosity to the plasma viscosity, shows a linear dependence of the pulse number n_p with α as shown in Figure 5-44.

$$n_p = 0.01a \tag{55}$$

In summary, the pulsatile inlet boundary condition has shown that surface tension and the parameter α, the ratio of the cytoplasm viscosity to the plasma viscosity, have major impact on the number of pulses needed to peel the cell away from the vessel wall while the parameter β, the ratio of the nucleus viscosity to the cytoplasm viscosity, has shown no impact on the number of the pulses needed to detach the cell for the inlet boundary conditions used in the present study.

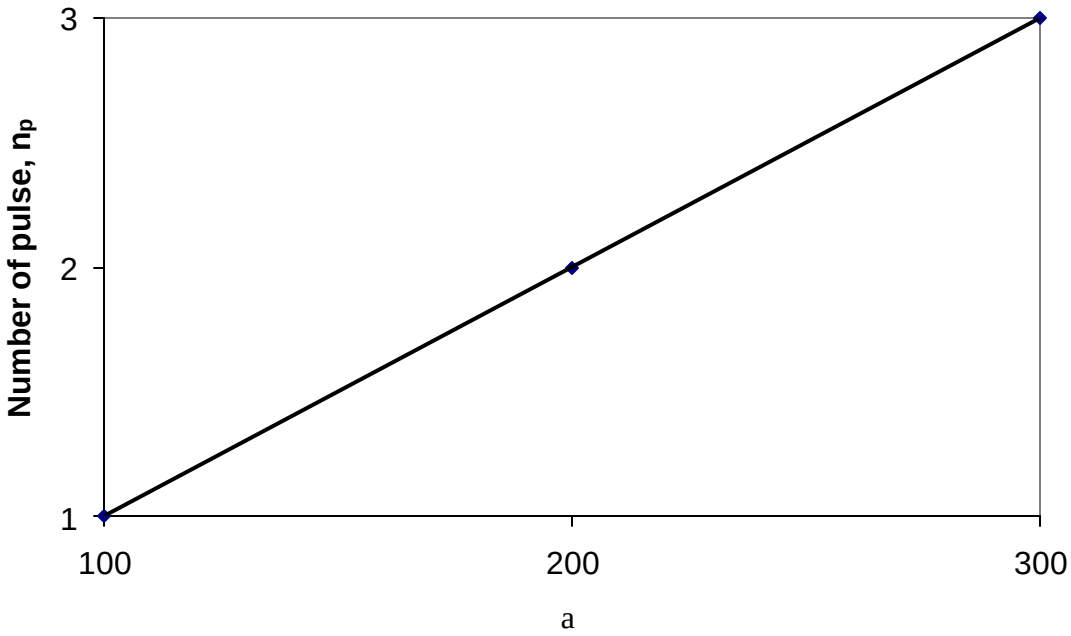

Figure 5-44: Effect of the parameter α on the number of pulses, n_p. $\bar{N}_r = 1.0$, $\bar{N}_l = 1.0$, $\bar{s} = 1.0$, $f_s = 0.2$, $b = 10$. The dot corresponds to the numerical results and the line is the curve fitting.

Effect of the Initial Bond Force

In all the previous computations, the initial bond force was taken to be zero, in the following computation; we assume an initial bond force, which varies with surface tension. The initial bond force is computed as follows:

$$F_{bo} = rg \tag{56}$$

where r is the cell radius and γ is the cell surface tension

Figure 5-45 shows a comparison of the peeling time for both non-zero and zero initial bond force for different values of surface tension. The peeling time is higher in the case of non-zero initial bond force. In most of the studies conducted over the past years, no initial bond force was assumed in the computation of the bond force.

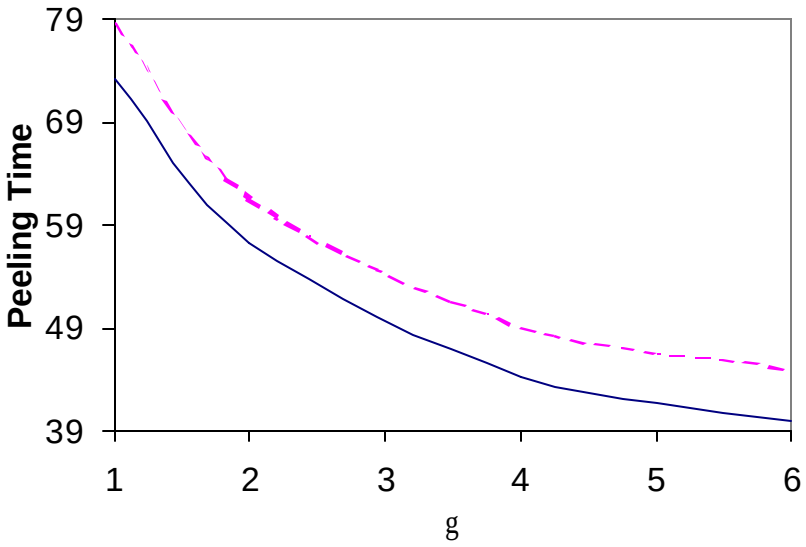

Figure 5-45: Comparison of peeling time for the zero (line) and non-zero (dashed line) initial bond force for different values of the surface tension. α = 100, $b = 10$, $\bar{N}_r = 1.0$, $\bar{N}_l = 1.0$, $f_s = 0.2$

CHAPTER 6
CONCLUSION AND DISCUSION

In this work, a multi-scale modeling for biofluid dynamics with an emphasis on cell adhesion was presented. This method breaks the computational work into two separate but interrelated domains. At the cellular level, a continuum model satisfying the field equations for momentum transfer and mass continuity was adopted. At the receptor-ligand or molecular level, a bond molecule was mechanically represented by a spring. A reversible two-body kinetic model characterized the association and dissociation of a bond. Communication between the macroscopic and microscopic scale models was facilitated interactively in the course of the computation.

The computational model was assessed using an adherent cell allowed to roll along the vessel wall under imposed shear flows. The cell was first modeled as a liquid drop with constant surface tension to illustrate the computational approach, and then as a compound drop in order to evaluate the effect of the nucleus. The results compare very well with those obtained computationally (Chang and Hammer, 2000;Dong et al., 1999; Dong and Lei, 2000; Tees et al., 2002) and experimentally (Patil et al., 2001; Schmidtke and Diamond, 2000). We have shown that cell deformability affects the rolling of a cell along a vessel wall. A cell with a higher surface tension rolls faster. These results are in agreement with those of Dong and Lei (2000), where only a small section of the membrane is allowed to deform.

The results also showed that as the shear rate increases, the bond lifetime decreases as observed by Alon et al. (1997, 1998) and Evans (1999), Schmidtke and Diamond (2000), Smith et al. (1999). The bond lifetime was also found to increase as the cell or nucleus viscosities increase. A decrease in cell diameter increases the peeling time and decreases the rolling velocity as observed by Tees et al. (2002) and Patil et al. (2001). We also studied the effect of vessel diameter on the adhesion process. We found that increasing the vessel diameter decreases the peeling time and increases the rolling velocity. In addition, we have shown that the peeling time is smaller for a pulsatile inlet condition than that of a uniform one and a non-zero initial bond force increases the peeling time. The bond lifetime was also shown to increase with the critical bond force, which is the force reaches by a bond molecule before breaking. An increase of the cell viscosity increases the critical bond force while increasing cell surface tension decreases the bond rupture force. In this work, we use the kinetic model proposed by Dembo et al. (1988), a drawback with this model is the assumption that the bonding stresses are the only distributed stresses acting on the membrane and bonds molecules are fixed on cell surface while Bell's model takes into account the role of the non specific potential forces in biological chemistry and the diffusion of the bond molecules to the contact area. Nontheless, the results obtained in this study won't be affected by the Bell's equation for the reverse reaction rate.

Many computational studies have considered the cell as a solid body. Some state that the deformation of the cell would not have a significant impact on rolling of the cell, but microvillus deformation is more important. However, the microvilli are connected to the cell surface; hence, a deformed microvillus also means cell deformation. The study

by N'Dri et al. (2002) has shown that a tether was pulled away from the cell membrane at high values of shear stress, but no membrane pulling was observed at low values of shear stress (Figure 5-15). These observations are consistent with what have been seen in the literature (Alon et al., 1997; Schmidtke and Diamond, 2000; Shao et al., 1998). Shao et al. (1998) have found that after the microvillus reaches its natural length, it will extend under a small pulling force or form a tether under a high pulling force. In addition, we have also observed a lifting of the cell from the vessel wall leading to its peeling as shown in Figure 5-2b. Similar observations were made by Sukumaran and Seifert (2001), who studied the influence of the shear flow on vesicles near a wall, and by Hodges and Jensen (2002) in their numerical study. The graph of the height of center of the cell above the plane increases rapidly with time, then reaches a plateau as observed in Figure 5-2b of the present study. In addition, in the study by Hodges and Jensen (2002), they found that changing the suspending fluid viscosity does not affect the rolling velocity of the cell along the wall. In their study, the viscosity of the cell was taken to be very small, so the fluid inside the cell was considered as invinscid. While in this study we have shown that fixing the suspending viscosity and varying either the cytoplasmic or/and the nucleus viscosity affect the rolling velocity of the cell showing that hydrodynamics do affect cell adhesion.

It is also known that a higher shear stress can enhance bond formation. How this phenomenon occurs is not clear. Does an increase of the shear stress increase first the diffusion and convection of bond molecules toward the contact area, or does an increase of the shear stress lead to an increase of the contact area due to cell deformation?

Although, in our study, bond formation is not considered *per se* due to the numerical resolution (we consider that a bond is formed when the distance between a receptor and ligand is less than a bond length, taken as $5x10^{-6}$cm), we can nevertheless comment from Figure 5-14 that an increase of the shear stress keeps the cell closer to the wall, and increases the contact area, as shown in Figure 5-15.

The finding of the present work is also consistent with the cell shape observed experimentally by Schmidtke and Diamond (2000) and numerically by Dong et al. (1999) and Dong and Lei (2000), who have shown that the cell goes from a spherical form to a tear-like drop shape.

Although the proposed approach was able to describe key features of cell adhesion, several issues still need to be addressed. For example, experimental results have shown that there is a threshold stress above which cell rolling occurs. However, the models proposed in the literature cannot capture this feature, indicating that the straightforward analogy between a bond molecule and a spring model is incomplete. A bond model with a yield force can be used to help resolve this deficiency. Furthermore, in the present study we have neglected membrane roughness and the effect of non-specific forces in the bond force computation. With respect to cell rheology, although the compound liquid drop model can capture most of the features of cell recovery and explain the reasons for the different published values for leukocyte viscosity, it does not include elastic effects which may be needed to fully describe leukocyte rheology (Tran-Son-Tay et al., 1994, 1998; Drury and Dembo, 1999, 2001; Kan et al., 1998, 1999). In addition, we assumed that the bond molecules are fixed on the membrane surface, which is not the case since bond molecules have been shown to diffuse laterally to the contact

area. The last issue is the assumption of a 2D cell model, which has some limitations such as force estimation with respect to 3D assumption.

Another issue is the error related to the multi-scale model. It is noted that the adhesion model is kinetics-based and is statistical. One approach to address the error associated with the micro-macro interactions is to consider the uncertainty of the microscopic prediction and assign a distribution function. This error distribution will then be incorporated into the adhesion model, based on which a statistical solution will be obtained, with the mean transmitted to the macroscopic model.

In order to compute the bond lifetime, we have assumed that bonds are broken if the cell travels 2 cell-radii based on non-physical cell shape beyond this distance. This assumption is solely based on cell mechanic and not on a single bond mechanic. To overcome this difficulty, we propose to use bond molecule strength as a condition for bond breakage. Therefore, the bond lifetime will be the unknown parameter that will depend on the hydrodynamic pulling force and the cell rheological properties.

Nevertheless, the present effort has offered a comprehensive framework to couple the cellular and the receptor-ligand dynamics and significant knowledge has been gained from this work. In the future, we will exploit the fact that the time scale for the formation of a new interface is fairly short, of the order on 1 nanosecond (ns) or less, and can therefore be tracked explicitly by large-scale parallel molecular dynamics simulations. Similar to the present model, the boundary conditions on the molecular simulation will be obtained from the continuum simulation and vice versa. It is simply a matter of time that a more comprehensive framework will be developed to offer new insights into the very complicated processes that occur in the dynamics of blood cells and blood flow.

LIST OF REFERENCES

Alon, R., Hammer D.A. and Springer T.A., 1995. Lifetime of the P-selectin-carbohydrate bond and its response to tensile force in hydrodynamic flow. *Nature (London)*, Vol. 374, pp 539-542

Alon R., Chen S., Puri K.D., Finger E.B. and Springer T.A., 1997. The kinetics of L-selectin tethers and the mechanics of selectin-mediated rolling. *J. Cell Biol.*, Vol. 38 (5), pp. 1169-1180.

Alon R., Chen S., Fuhlbrigge R., Puri K.D. and Springer T.A., 1998. The kinetics and shear threshold of transient and rolling interactions of L-selectin with its ligand on leukocytes, *Proc. Natl. Acad. Sci. USA*, Vol. 95, pp. 11631-11636.

Bell, G.I., 1978. Models for the specific adhesion of cells to cells, *Science,* Vol. 200, pp. 618-627.

Bell, G., Dembo, M., and Bongrand, P. 1984. Cell adhesion: Competition between nonspecific repulsion and specific bonding. *Biophys. J.* Vol. 45, pp. 1051-1064.

Brunk, D.K., Goetz, D.J. and Hammer D.A., 1996. Sialyl Lewis(x)/E-selectin-mediated rolling in a cell-free system. *Biophys. J.* Vol. 71, pp. 2902-2907.

Brunk, D.K. and Hammer D.A., 1997. Quantifying rolling adhesion with a cell-free assay: E-selectin and its carbohydrate ligands. *Biophys. J.*, Vol. 72, pp. 2820-2833.

Chang, K.C., Tees, D.F.J. and Hammer, D.A., 2000. The state diagram for cell adhesion under flow: Leukocyte rolling and firm adhesion. *Proc. Natl. Acad. Sci. USA*, Vol. 97, pp. 11262-11267.

Cheng Zhu, 2000. Kinetics and mechanics of cell adhesion. *J. Biomechanics,* Vol. 33, pp. 23-33.

Chen S. and Springer T.A., 1999. An automatic breaking system that stabilizes leukocyte rolling by an increase in selectin bond number with shear. *J. Cell Biol.*, Vol. 144, pp. 185-200.

Chen S. and Springer T.A., 2001. Selectin receptor-ligand bonds: Formation limited by shear rate and dissociation governed by Bell model. *Proc. Natl. Acad. Sci. USA*, Vol. 98, pp. 950-955.

Cozens-Roberts, C., Lauffenburger, D. A. and Quinn, J. A. 1990. A receptor-mediated cell attachment and detachment kinetics; I. Probabilistic model and analysis. *Biophys. J.*, Vol. 58, pp. 841-856.

Dembo, M., Torney, D. C., Saxaman, K. and Hammer, D., 1988. The reaction-limited kinetics of membrane-to-surface adhesion and detachment. *Proc. R. Soc. Lon. B,* Vol. 234, pp. 55-83.

Demerdzic, I. and Peric, M., 1990. Finite volume method for prediction of fluid flow in arbitrary shaped domains with moving boundaries. *Int. J. Numer. Meths. Fluids*, Vol. 10, pp. 771-790.

Dong, C., Cheng, Cao, J., Struble, E.J. and Lipowsky, H.H., 1999. Mechanics of leukocyte deformation and adhesion to endothelium in shear flow. *Ann. Biomed. Eng.*, Vol. 23, pp. 322-331.

Dong, C. and Lei X.X. 2000. Biomechanics of cell rolling: shear flow, cell-surface adhesion, and cell deformability. *J. Biomechanics*, Vol. 33, pp. 35-43

Drury J.L. and Dembo M. 1999. Hydrodynamics of micropipette aspiration. *Biophys J.* 76:110-128.

Drury J.L. and Dembo M. 2001. Aspiration of human neutrophils: Effect of shear thinning and cortical dissipation. *Biophys J.* 81:3166-3177.

Evans, E.A., 1983. Bending elastic modulus of red blood cell membrane derived from buckling instability in micropipet aspiration tests. *Biophys J.*, Vol. 43, pp. 27-30.

Evans, E.A., 1985a. Detailed mechanics of membrane-membrane adhesion and separation. I. Continuum of molecular cross-bridges. *Biophys. J.*, Vol. 48, pp. 175-183.

Evans, E.A., 1985b. Detailed mechanics of membrane-membrane adhesion and separation. II. Discrete kinetically trapped molecular bridges. *Biophys*. J., Vol. 48, pp. 185-192.

Evans, E., and Yeung, A., 1989. Apparent viscosity and cortical tension of blood granulocytes determined by micropipet aspiration. *Biophys. J.*, Vol. 56, pp. 151-160.

Evans E., 1999. Looking inside molecular bonds at biological interfaces with dynamic force spectroscopy. *Biophys. Chem.*, Vol. 82, pp. 83-97.

Fauci L.J. and Peskin C.S., 1988. A computational model of aquatic animal locomotion. *J. Comput. Phys.*, Vol. 77, pp. 85-108.

Fry D. L., 1987. Mass transport, atherogenesis and risk. *Arteriosclerosis*, Vol. 7, pp. 88-100.

Giddens D. P., Zarins C. K. and Glagov S., 1993. The role of fluid mechanics in the localization and detection of atherosclerosis. *J. Biomech. Eng*., Vol. 115, pp. 588-594.

Goldman A.J., Cox R.G. and Brenner H., 1967a. Slow motion of a sphere parallel to a plane wall-I: Motion through a quiescent fluid. *Chemical Eng. Sc.*, Vol. 22, pp. 637-651

Goldman A.J., Cox R.G. and Brenner H., 1967b. Slow motion of a sphere parallel to a plane wall-II: Couette flow. *Chemical Eng. Sc.*, Vol. 22, pp. 653-660.

Greenberg A.W., Brunk D.K. and Hammer D.A., 2000. Cell-Free rolling mediated by L-selectin and sialyl Lewisx reveals the shear threshold effect. *Biophys. J.*, Vol. 79, pp. 2391-2402.

Gyton, A., 1986. *Textbook of Medical Physiology*. Philadelphia: Saunders (7^{th} Edn.)

Hammer, D. A. and Lauffenburger, D. A., 1987. A dynamical model for receptor-mediated cell adhesion to surfaces. *Biophys. J*., Vol. 52, pp. 475-487.

Hammer, D. A. and Apte S. M., 1992. Simulation of cell rolling and adhesion on surfaces in shear flow: General results and analysis of selectin-mediated neutrophil adhesion. *Biophys. J*., Vol. 63, pp. 35-57.

Hammer, D. A. and Tirrell, M., 1996. Biological adhesion at interfaces. *Annu. Rev. Mater. Sci.*, Vol. 26, pp. 651-691.

Hochmuth R.M., Ting-Beall H.P., Beat B.B., Needham D. and Tran-Son-Tay R., 1993. The viscosity of passive human neutrophils undergoing small deformations. *Biophys. J.*, Vol. 64, pp. 1596-1601.

Hodges S. R. and Jensen O. E., 2002. Spreading and peeling dynamics in a model of cell adhesion, *J. Fluid. Mech.*, Vol. 460, pp. 381-409.

Jin S., Oshinski J. and Giddens D., 2001. Effects of inflow conditions and wall motion on flow in the ascending aorta, *Proc. of the Bioengineering Conference ASME, BED*-Vol. 50, pp. 13-14.

Juric D. and Tryggvason G., 1996. A front tracking method for dendritic solidification. *J. Comp Phys.*, Vol. 123, pp. 127-148.

Kan H.-C., Udaykumar H.S., Shyy W. and Tran-Son-Tay R.,1999a. Numerical analysis of the deformation of an adherent drop under shear flow. *J. Biomech. Eng*., Vol. 121, pp. 160-169.

Kan H.-C., Udaykumar H. S., Shyy W., Vigneron P. and Tran-Son-Tay R., 1999b. Effects of nucleus on leukocyte recovery. *Ann. Biomed. Eng.* Vol. 27, pp. 648-655.

Kan H.-C., Udaykumar H.S., Shyy W. and Tran-Son-Tay R.,1998. Hydrodynamics of a compound drop with application to leukocyte modeling. *Phys. Fluids*, Vol. 10, pp. 760-774.

Kaplanski G., Farnarier C., Tissot O., Pierres A., Benoliel A.-M., Alessi M.C., Kaplanski S. and Bongrand P., 1993. Granulocyte-endothelium initial adhesion: Analysis of transient binding events mediated by E-selectin in a laminar shear flow. *Biophys. J.*, Vol. 64, pp. 1922-1933.

Kitano, T., Yutani Y., Shimazu, A., Yano, I., Ohashi, H. and Yamano, Y., 1996. The role of physicochemical properies of biomaterials and bacterial cell adhesion in vitro". *Int. J. Artif. Organs*, Vol. 19, pp. 353-358.

Kilner P.J., Yang G.Z., Mohiaddin R.H., Firmin D.N. and Longmore D.B., 1993. Helical and retrograde secondary flow patterns in the aortic arch studied by three-directional magnetic resonance velocity mapping. *Circulation*, Vol. 88, pp. 2235-2247.

Kuo S. C., Hammer D.A. and Lauffenburger D.A., 1997. Simulation of detachment of specifically bound particles from surfaces by shear flow. *Biophys. J.*, Vol. 73, pp. 517-531.

Kwak S. and Pozrikidis C, 1998. Adaptive triangulation of evolving, closed or open surfaces by advancing-front method. *J. Comput. Phys.*, Vol. 145, pp. 61-88.

Lauffenburger, D.A. and Linderman, J.J., 1993. *Receptors: Models for Binding, Trafficking, and Signaling*. Oxford University Press, New York.

Lawrence, M.B. and T.A. Springer, 1991. Leukocytes roll on a selectin at physiologic flow rates: distinction from and prerequisite for adhesion through integrins. *Cell*, Vol. *65*, pp. 859-873.

Liu H., 2000. Computation of the vortical flow in human aorta. *Proceedings of the ASME, Fluids Engineering Division*, FED-Vol. 253, pp. 497-502.

Long, M.W., 1995. Tissue microenvironments. In J.D. Bronzino (editor): *The Biomedical Engineering Handbook*, Boca Raton, FL: CRC Press, Chap. 114, pp. 1692-1709.

N'Dri, N., Shyy, W., Tran-Son-Tay, R. and Udaykumar, H.S., 2000. A multi-scale model for cell adhesion and deformation. *ASME IMECE Conference*. FED -Vol. 253, 205-213.

N'Dri, N., Shyy, W. and Tran-Son-Tay, R. (submitted). Computational modeling of cell adhesion and movement using a continuum-kinetics approach.

N'Dri N., Shyy W., Liu H., Tran-Son-Tay R. (in press). Multi-Scale modeling spanning receptor, cell and blood vessel scales.

Pedley T.J., 1980. *The Fluid Mechanics of Large Vessels*. Cambridge: Cambridge University Press.

Peskin C. S., 1977. Numerical analysis of blood flow in the heart. *J. Comput. Phys.*, Vol. 25, pp 220-252.

Ramachandran V., Nollert M.U., Qiu H., Liu W.J., Cummings R.D., Zhu C., and McEver R.P., 1999. Tyrosine replacement in P-selectin glycoprotein ligand-1 affects distinct kinetic and mechanical properties of bonds with P- and L-selectin. *Proc. Natl. Acad. Sci. USA*, Vol. 96, pp. 13771-13776.

Schmid-Schönbein G.W., Fung Y.and Zweifach B.W., 1975. Vascular endothelium-leukocyte Interactions: Sticking shear force in venules. *Circ. Res.*, Vol. 36, pp. 173-184.

Schmid-Schonbein G. W., Shih Y. Y., Chien S., 1980. Morphometry of human leukocytes. Blood, Vol. 56, pp. 866-875.

Schmidtke D.W. and Diamond S.L., 2000. Direct observation of membrane tethers formed during neutrophil attachment to platelets or P-selectin under physiological flow. *J. Cell Biol.*, Vol. 149 (3), pp. 719-729.

Shao J.-Y. and Hochmuth R.M., 1996. Micropipette suction for measuring piconewton forces of adhesion and tether formation from neutrophil membranes. *Biophys. J.*, Vol. 71, pp. 2892-2901.

Shao J.-Y., Ping Ting-Beall H., Hochmuth R.M., 1998. Static and dynamic lengths of neutrophil microvilli. *Proc. Natl. Acad. Sci. USA*, Vol. 95, pp. 6797-6802.

Shao J.-Y. and Hochmuth R.M., 1999. Mechanical anchoring strength of L-selectin, β2 integrins, and CD45 to neutrophil cytoskeleton and membrane. *Biophys. J.*, Vol. 77, pp. 587-596.

Shinde Patil V.R., Campbell C.J., Yun Y.H., Slack S.M. and Goetz D.J., 2001. Particle diameter influences adhesion under flow. *Biophys. J.*, Vol. 80, pp. 1733-1743.

Shyy W., 1994. *Computational Modeling for Fluid Flow and Interfacial Transport*. Amsterdam, The Netherlands: Elsevier Science Publishers B.V.

Shyy W., Udaykumar H. S., Rao M. M. and Smith R.W., 1996. *Computational Fluid Dynamics with Moving Boundaries*. Washington, D.C.: Taylor & Francis.

Shyy W., Francois M., Udaykumar H.S., N'Dri N. and Tran-Son-Tay R., 2001. Moving Boundaries in micro-scale biofluid dynamics. *Applied Mechanics Reviews*, Vol. 5, no5, pp 405-453.

Skalak R., 1972. *Mechanics of the Microcirculation, Biomechanics: Its Foundation and Objectives*. Edited by Y.C. Fung, N. Perrone and M. Anliker, Englewood Cliffs, New Jersey: Prentice-Hall.

Smith Mcrae J. Berg E.L. and Lawrence M.B., 1999. A direct comparison of selectin-mediated transient, adhesive events using high temporal resolution. *Biophys. J.*, Vol. 77, pp. 3371-3383

Springer, T.A., 1990. Adhesion receptors of the immune system. *Nature*, Vol. 346, pp 425-434.

Sukumaran S. and Seifert U., 2001. Influence of shear flow on vesicles near a wall: a numerical study. *Phys. Rev. E 64*, 011916-1-011916-11.

Tees D.F.J., Chang K.C., Rodgers S.D. and Hammer D.A., 2002. Simulation of cell adhesion to bioreactive surfaces in shear: The effect of cell size. *Ind. Eng. Chem. Res.*, Vol. 41, pp. 486-493.

Thomas P.D. and Lombard C.K., 1979. Geometric conservation law and its application to flow computations on moving grids. *AIAA J.*, Vol. 15, pp. 226-243.

Thompson, J.F., Warsi, Z.U.A. and Mastin, C.W., 1985. *Numerical Grid Generation*. New York: Elsevier.

Tran-Son-Tay R., N'Dri N., Shyy W. (in press). Micro-Nano Coupling in Biological Systems.

Tran-Son-Tay, R., Ting-Beall H. P., Zhelev D. V., and Hochmuth R. M. 1994. Viscous behavior of leukocytes. In Cell Mechanics and Cellular Engineering, V. C. Mow, F. Guilak, R. Tran-Son-Tay, and R. M. Hochmuth, Eds. Springer-Verlag. 22-32.

Tran-Son-Tay, R., Kan H.-C., Udaykumar H. S., and Shyy W. 1998. Rheological modeling of leukocytes. *Medical & Biological Engineering & Computing*, Vol. 36, pp. 246-2508.

Udaykumar H.S., Kan H.-C., Shyy W. and Tran-Son-Tay R., 1997. Multiphase dynamics in arbitrary geometries on fixed Cartesian grids. *J. Comput. Phys.*, Vol. 137, pp. 366-405.

Udaykumar H.S., Mittal R. and Shyy W., 1999. Computation of solid-liquid phase fronts in the sharp interface limit on fixed grids. *J. Comput. Phys.*, Vol. 153, pp. 535-574.

Unverdi S.O. and Tryggvason G., 1992. A front tracking method for viscous, incompressible, multi-fluid flows. *J. Comput. Phys.*, Vol. 100, pp. 25-37.

Ye T., Mittal R., Udaykumar H.S., and Shyy W., 1999. A Cartesian grid method for simulation of viscous incompressible flow with complex immersed boundaries. *J. Comput. Phys.*, Vol. 156, pp. 209-240.

Ye T., Shyy W., and Chung J. N., 2001. A Fixed-Grid, Sharp-Interface Method for Bubble Dynamics and Phase Change. *J. Comput. Phys.*, Vol. 174, pp.781–815.

Ward, M.D., Dembo, M. and Hammer, D.A., 1995. Kinetics of cell detachment: effect of ligand density. *Annals Biomed. Eng.*, Vol. 23, pp. 322-331.

Weiss, L., 1990. Metastatic inefficiency. *Adv. Can. Res*., Vol. 54, pp. 159-211.

BIOGRAPHICAL SKETCH

Narcisse Abou N'Dri was born in Ivory Coast (Cote d'Ivoire) where he received his bachelor's degree in applied mathematics at the University of Cocody. Then, he earned a fellowship from his government to pursue his study in France. After graduating with a doctoral degree in biorheology at the University of Paris 6, he decided to complete his academic training by expanding his knowledge in computational fluid dynamics. He entered the PhD program at the University of Florida in 1999.